

Atmospheric pressure dielectric barrier discharges interacting with liquid covered tissue

Wei Tian¹ and Mark J Kushner^{2,3}

¹ University of Michigan, Department of Nuclear Engineering and Radiological Science, 2355 Bonisteel Boulevard, Ann Arbor, MI 48109-2104, USA

² University of Michigan, Department of Electrical Engineering and Computer Science, 1301 Beal Avenue, Ann Arbor, MI 48109-2122, USA

E-mail: bucktian@umich.edu and mjkush@umich.edu

Received 15 January 2014, revised 19 February 2014

Accepted for publication 25 February 2014

Published 3 April 2014

Abstract

The interaction of plasmas with liquids is of increasing importance in biomedical applications. Tissues treated by atmospheric pressure dielectric barrier discharges (DBDs) in plasma medicine are often covered by a thin layer of liquid, typically a blood serum like water with dissolved gases and proteins up to hundreds of micrometres thick. The liquid processes the plasma-produced radicals and ions prior to their reaching the tissue. In this paper, we report on a computational investigation of the interaction of DBDs in humid air with a thin water layer covering tissue. The water layer, 50–400 μm thick, contains dissolved $\text{O}_{2\text{aq}}$ (aq means an aqueous species) and alkane-like hydrocarbons (RH_{aq}). In the model, the DBDs are operated with multiple pulses at 100 Hz followed by a 1 s afterglow. Gas phase reactive oxygen and nitrogen species (RONS) intersect the water-vapour saturated air above the liquid and then solvate when reaching the water. The photolysis of water by plasma-produced UV/VUV plays a significant role in the production of radicals. Without RH_{aq} , $\text{O}_{2\text{aq}}^-$, $\text{ONOO}_{\text{aq}}^-$, $\text{NO}_{3\text{aq}}^-$ and hydronium ($\text{H}_3\text{O}_{\text{aq}}^+$) dominate the water ions with $\text{H}_3\text{O}_{\text{aq}}^+$ determining the pH. The dominant RONS in the liquid are $\text{O}_{3\text{aq}}$, $\text{H}_2\text{O}_{2\text{aq}}$, and $\text{HNO}_{x\text{aq}}$. Dissolved $\text{O}_{2\text{aq}}$ assists the production of $\text{HNO}_{3\text{aq}}$ and HOONO_{aq} during the afterglow. With RH_{aq} , reactive oxygen species are largely consumed, leaving an $\text{R}_{\text{aq}}\cdot$ (alkyl radical) to reach the tissue. These results are sensitive to the thickness of the water layer.

Keywords: dielectric barrier discharge, plasmas on liquids, atmospheric pressure plasma, plasma medicine

(Some figures may appear in colour only in the online journal)

1. Introduction

Atmospheric pressure plasmas (APPs) are being investigated for use in healthcare [1–3] and the environmental remediation of toxic substances [4–6]. Dielectric barrier discharges (DBDs) are one preferred APP due to their intrinsic stability against arcing [7]. In environmental applications, DBDs have been implemented for nitrogen-oxide (N_xO_y) removal from exhausts and in the removal of volatile organic compounds (VOCs) from gases [8–10]. In healthcare, DBDs have been investigated for the treatment of human tissue in the context

of wound healing and for killing bacteria for the sterilization of surfaces [11–13]. The use of APPs for wound healing and skin treatment is still at an early stage, and is an active area of research in which clinical studies are in progress [14, 15]. Many such applications involve DBDs (or other plasmas) in contact with liquids, either intentionally as in the purification of water or coincidentally as in the treatment of wounds. Most wounds in their early stages are covered with a water-like liquid resembling blood serum being 93% water and 7% proteins [16]. The thickness of the liquid layer is typically a few hundred micrometres. The plasma-produced reactive fluxes first react with the hundreds-of-micrometres-thick liquid

³ Author to whom any correspondence should be addressed.

layer. The liquid then acts as a filter, which modifies the plasma-produced fluxes prior to those fluxes or their reaction products reaching the underlying tissue. The mechanisms for APPs delivering reactivity through the liquid layer to the tissue below are not clear.

There is a prior body of work on plasma formation in liquids in the context of electrical breakdown [17, 18] and from the environmental science community for organic compound removal from water by, for example, electron beam injection [19, 20]. There are also works in atmospheric chemistry which address the formation of acidic aerosols from atmospheric N_xO_y [21, 22]. The recent interest in plasma medicine has motivated works investigating *plasmas-onto-water* (POW). For example, *plasma-activated-water* (PAW) results from indirect or direct exposure of water to APPs [23–25]. This process results in the water having long-lived biocidal properties [23], which have been attributed to the formation of, for example, peroxy nitrates [25]. More general studies of POW have investigated the formation of acids, reactive oxygen species (ROS) and reactive nitrogen species (RNS).

The biological implications of plasmas on liquids is an active area of research. There are two general configurations. The first configuration is a remote plasma, either a DBD or plasma jet, where the ionized gas is not in direct contact with the surface of the liquid. Reactivity is produced in the liquid as a consequence of diffusion into the liquid of gas phase species created some distance away. The second configuration is a direct plasma where the ionized gas is in direct contact with the liquid, also either a DBD or a plasma jet. Here, reactivity is additionally produced by electrons and ions directly solvating into the liquid, and by photolysis of the liquid by UV and VUV photons produced by the plasma. The focus of this paper is a direct DBD plasma in contact with water.

The typical DBD used to treat tissue or wounds consists of a powered electrode covered by an insulator. The treated tissue is separated from the dielectric by a few mm, and serves as a floating electrode [11]. The tissue is often covered by a liquid layer, which is typically hundreds of micrometres thick. The liquid is mostly water, which may contain dissolved gases such as O_{2aq} or CO_{2aq} , and organic compounds such as proteins as contained in blood serum [16]. (The subscript $_{aq}$ denotes an aqueous species.) In this configuration, the liquid layer is directly exposed to the chemically reactive neutral radicals, electrons, ions and UV/VUV radiation produced by the plasma.

The discharge becomes more complex when considering the coupled plasma-liquid system. From simply a circuit perspective, the liquid is a lossy dielectric which contributes to the series capacitance of the DBD and so contributes to power loss. The liquid surface, water in our case, evaporates vapour to humidify the air, more so closer to the surface. The locally more humid air changes the plasma characteristics, particularly with respect to the production of hydroxyl radicals. Once radicals and ions either diffuse into or are formed in the water (that is, solvated species), a second hierarchy of reactions begins. The duration of an individual plasma filament in the DBD is relatively short—from a few to tens of ns. Many water related reactions, such as the solvation of electrons and

charge exchange, have similarly short (or shorter) timescales. However, the reaction chain initiated in the water by the plasma can evolve over seconds to minutes. For example, hydrogen peroxide, H_2O_{2aq} , is formed by the reaction of two hydroxyl radicals, OH_{aq} , which result from OH solvating into the water. Aqueous ozone, O_{3aq} , is formed through the solvation of gaseous O_3 . Both H_2O_{2aq} and O_{3aq} can persist in the water for up to days. These long-lived species in part explain why PAW maintains its chemical reactivity for long times after exposure to plasma [23, 26].

These processes have recently been investigated using global modelling [27–29]. Bruggeman and co-workers [27] reported that the RNS play a more important role than ROS (with the exception of H_2O_{2aq}) in bacteria killing in their experiment. They used a zero-dimensional solution kinetics model to address the aqueous reactions. The simulations showed a clear distinction between short-lived species such as HO_{2aq} and OH_{aq} and long-lived species such as H_2O_{2aq} and NO_{3aq}^- . The nitrate, NO_{3aq}^- , and nitrite, NO_{2aq}^- , concentrations were measured to be $1 \times 10^{-4}M$ and $8 \times 10^{-6}M$, respectively, after 60 s of treatment. (Here $M \equiv$ mole/litre. Note that a concentration of $1 \times 10^{-4}M$ in water corresponds to $6 \times 10^{16} \text{ cm}^{-3}$.) The experiments also showed the difference between intermediate species such as O_{2aq}^- , O_{aq}^- , OH_{aq} , which only survive for milliseconds after plasma treatment, and stable species such as $ONOO_{aq}^-$, NO_{3aq}^- , H_2O_{2aq} , which are the terminal species. In their measurement, H_2O_{2aq} is about $5 \times 10^{-4} \text{ mole}^{-1} \text{ l}^{-1}$ after plasma treatment.

Hamaguchi [28] also developed a global model to investigate plasma-initiated electrochemistry in water. With only OH fluxes onto the water, the results of his model showed a rapid conversion of OH_{aq} radicals to H_2O_{2aq} , with a rate coefficient of $4.5 \times 10^9 M^{-1} s^{-1}$. H_2O_{2aq} is then a terminal species which persists for seconds. With additional fluxes of NO onto the water, dissolved NO_{aq} and OH_{aq} produce a large variety of reactive species, such as NO_{3aq}^- , $ONOO_{aq}^-$ and O_{2aq}^- . The results of the model indicated that acidification of the water is due to the generation of nitric acid.

Lukes and co-workers [29] experimentally investigated the formation of aqueous radicals in non-buffered and buffered water by transient spark discharges, which are basically corona discharges. Non-acidic buffered environments resulted in higher concentrations of nitrites, NO_{2aq}^- ($\approx 6 \times 10^{-4}M$), and slightly lower concentrations of H_2O_{2aq} ($\approx 4 \times 10^{-4}M$) compared to non-buffered water, with concentrations of nitrites ($2 \times 10^{-4}M$) and H_2O_{2aq} ($7 \times 10^{-4}M$). The concentration of nitrates, NO_{3aq}^- , was not significantly affected by the buffering. The concentration of peroxy nitrates, $ONOO_{aq}^-$, was qualitatively estimated to be of the order of $10^{-6}M$, and is believed to play an important role in bacterial inactivation. Ozone also contributes to the bacterial inactivation and is more important in non-acidic environments, such as buffered water.

In this paper, we report on results from a two-dimensional computational investigation of DBDs in contact with water-covered tissue. A three-pulse negative discharge and its 1–20 s afterglow is investigated in both the gas phase and liquid phase. The underlying tissue is modelled as a dielectric material with no conductivity. The liquid layer is treated identically

to the gas as a partially ionized substance but with a higher density and specified permittivity. So from a computational perspective, the same equations (e.g., continuity, energy, radiation transport, Poisson's equation) are solved both in the gas phase and the liquid phase, albeit with different species and reaction mechanisms.

In the DBDs, the gas phase plasma is produced with multiple -18 kV pulses at 100 Hz followed by a 1 s afterglow in most cases. Reactive oxygen and nitrogen species (RONS) produced in the gas phase intersect the water-vapour-saturated air above the liquid and then solvate when reaching the liquid. Photoionization and photodissociation of the water by the plasma-produced UV/VUV radiation plays a significant role in radical production. Pure water, water with dissolved O_{2aq} and water with a generic hydrocarbon alkane, RH_{aq} , were investigated. Without RH_{aq} , O_{2aq}^- , $ONOO_{aq}^-$, NO_{3aq}^- and hydronium ($H_3O_{aq}^+$) dominate the water ions, with $H_3O_{aq}^+$ determining the pH. The dominant RONS in the liquid are O_{3aq} , H_2O_{2aq} and $HNO_{x, aq}$. The formation of $HOONO_{aq}$ is also included since $HOONO_{aq}$ has a high oxidizing potential. For liquids containing RH_{aq} , the ROS are largely consumed, leaving R_{aq} (alkyl radical) to reach the tissue.

The model used in this investigation is described in section 2, followed by a discussion of simulated DBDs in contact with a thin water layer in section 3. Our concluding remarks are in section 4.

2. Description of the model

The model used in this investigation is *nonPDPSIM* and the gas phase portions of the model are described in detail in [30, 31]. Briefly, *nonPDPSIM* is a two-dimensional simulation performed on an unstructured numerical mesh in which Poisson's equation, transport equations for charged and neutral species, the electron energy conservation equation and radiation transport are solved by direct time integration. Boltzmann's equation is solved for electron transport and rate coefficients, which are tabulated as a function of the average electron energy and are interpolated during the execution of the model. A Green's function propagator is used for radiation transport and photon-induced ionization and dissociation.

In extending *nonPDPSIM* to the liquid phase, we attempted to make a minimum of limiting assumptions. The numerical mesh is divided into zones that are specified as being gas or liquid. Computationally and algorithmically, the liquid zone is treated identically to the gas phase. The same equations (e.g., Poisson's, transport and energy conservation, radiation transport) are solved in the liquid as in the gas. In order to properly include the larger dielectric constant of the liquid, an atomic polarizability is specified for each species so that the number density weighted polarizability yields the proper dielectric constant. Transport coefficients for neutral and charged species, and absorption cross-sections, are determined by the local densities on a mesh-point-by-mesh-point basis.

The rate of transport of gas phase species into the liquid is determined by Henry's law considerations [32, 33]. Henry's law states that at a constant temperature and at equilibrium, the density of a gas dissolved in a liquid, water in this case,

Table 1. Dimensionless Henry's law constants for various species at 300 K and 1 atm [32, 33].

Species	Henry's law constant
OH	6.92×10^2
H_2O_2	1.92×10^6
O_3	3×10^{-1}
NO	4.4×10^{-2}
NO_2	2.8×10^{-1}
NO_3	4.15×10^1
N_2O_3	6×10^2
N_2O_4	3.69×10^1
N_2O_5	4.85×10^1
HNO_2	1.15×10^3
HNO_3	4.8×10^6
HOONO	4.8×10^{6a}

^a Approximated by analogy to HNO_3 .

is proportional to the partial pressure of the gas in the vapour phase. Proportionality constants for use in Henry's law for water are shown in table 1. A larger Henry's law constant indicates a greater likelihood that the species in contact with water will dissolve into the liquid. For example, H_2O_2 and HNO_3 are quickly solvated in water, while the solvation process for NO and O_3 is slow. Henry's law was implemented into *nonPDPSIM* in the following manner. The interface between the gas and liquid phases is located by determining the liquid mesh points, j , that have gas phase mesh points, i , as at least one neighbour. For diffusive transport from the gas into the liquid, the diffusion coefficient between i and j is given by

$$D_{ij} = D_i \left(\frac{hn_i - n_j}{hn_i} \right), \quad (1)$$

where D_i is the diffusion coefficient in the gas phase, n_i and n_j are the densities of the species in the gas and water, and h is Henry's law constant. This effectively shuts off diffusion into the water when the equilibrium density at the surface is reached.

Due to their higher potential energies, we assumed that all ions, as well as electrons, pass directly into the liquid. That is, the liquid mesh point having a gas phase mesh point as a neighbour receives charged gas species with a rate of diffusion (or drift in the electric field) given by their gas phase transport coefficients. For transport of the charged species out of the liquid into the gas, the liquid transport coefficients are used, which effectively traps the charged species in the liquid. From a practical perspective, the diffusion out of the water of dissolved gas phase ions or electrons is highly unlikely since their rates of solvation or charge exchange are large.

The exception to these practices is the evaporation of the water. We do not explicitly address the surface tension of the water-gas interface. Instead, we assume that the gas phase density of water at the liquid surface is given by its saturated vapour pressure, which is 27 Torr at 300 K. The corresponding water vapour density is then used as a boundary value for diffusion of water vapour from the interface into the gas.

Radiation transport is addressed in the same manner as described in [30, 31], while accounting for local values of absorption cross-sections and densities of either gas or liquid

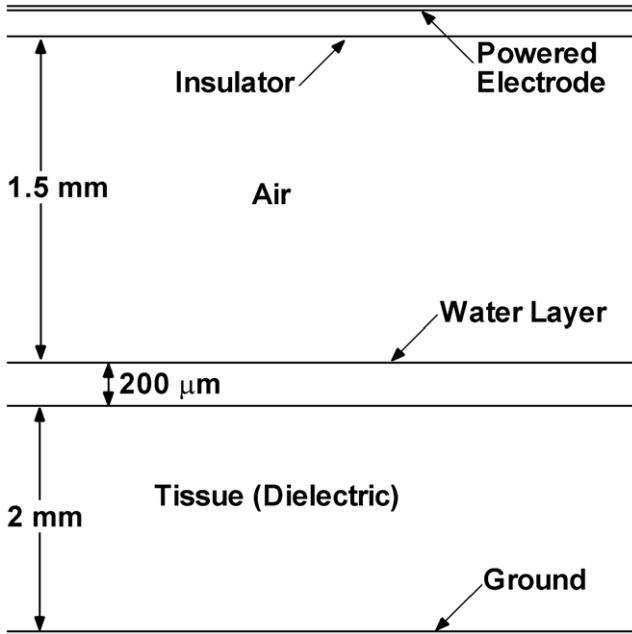


Figure 1. Schematic of the geometry where the plasma filament propagates. The total computational domain is 4 mm × 4 mm.

phase species. For example, the photon flux originating from emission by species k at mesh point i arriving at mesh point j is given by

$$\phi_k(\vec{r}_j) = A_k N_k(\vec{r}_i) \exp\left(-\int_{r_i}^{r_j} \sum_m N_m(\vec{r}') \sigma_{km} d\vec{r}'\right) \times f(\vec{r}_i, \vec{r}_j) \quad (2)$$

where N_k is the density of the emitting species having the Einstein coefficient A_k , the sum is over the absorbing species having density N_m and the absorption cross-section σ_{km} , and f is a function to account for the reduction in flux due to obscurations and expansion of the photon front, which has a different form for a specific coordinate system. The integral accounts for absorption along the trajectory of the photon, which naturally accounts for the transition from the gas phase into the water. We do not account for the refraction of light at the boundary of the gas–liquid interface. Although refraction is important for photons that have a long mean free path in the water, for the results discussed here, we only considered transport of UV and VUV capable of photolysing or photoionizing the water. From a practical perspective, the mean free path for these photons in the water is only a few to 10 μm , and so the change in their direction due to refraction is not important.

The Cartesian geometry used in this investigation is shown in figure 1. The left and right boundaries (not shown in figure 1) use reflective boundary conditions and are placed sufficiently far away that they do not influence the calculation. (The full width of the computational domain is 4 mm.) The powered electrode is at the top and is covered by a dielectric 0.12 mm thick with a dielectric constant of $\varepsilon/\varepsilon_0 = 3$. The gap between the dielectric and the surface of the water is 1.5 mm and is initially filled with humid air. The tissue at the bottom of the domain is 2 mm thick and is represented as a dielectric with a relative permittivity of $\varepsilon/\varepsilon_0 = 5$ and no conductivity.

An electrical ground plane is below the tissue. The tissue is covered by a water layer with $\varepsilon/\varepsilon_0 = 80$, and is 200 μm thick in the base case. The numerical grid consists of 10 526 nodes and 20 747 volume elements, of which 8681 nodes and 17 225 volume elements are in the plasma region in the gas and liquid layer. The volume near the liquid–gas interface is refined with smaller dimensions, about 20 μm compared to 50 μm in the remote gas gap. This mesh spacing will not resolve the dynamics of double layers or other charge layers that may form at the surface of the liquid, as these structures may be as thin as a few nm [34].

The liquid is basically water with dissolved oxygen $\text{O}_{2\text{aq}}$ of 8 ppm [35] at room temperature and under atmospheric pressure. We have not considered any initial conductivity of the liquid as may occur in many biological liquids due to the presence of electrolytes. The change in conductivity of the liquid that results from the plasma treatment is self-consistently accounted for through the evolution of the ion content of the liquid and the resulting charge density that is included in the solution of Poisson’s equation. The reaction mechanism in the water was developed from the environmental science literature [36], and is shown in table 2.

The VUV/UV radiation generated by high lying excited states of N_2 is attenuated by absorption in propagating through the plasma and into the water or onto solid surfaces [40]. In this model, photons are emitted from the highly excited states of N_2 , involving $\text{N}_2(b')$ with an energy of 12.8 eV and $\text{N}_2(c')$ with an energy of 12.9 eV. O_2 in the gas phase undergoes ionization and $\text{H}_2\text{O}_{\text{aq}}$ undergoes both ionization and dissociation.

Three discharge pulses in the air gap at 100 Hz are simulated followed by a 1 s afterglow for the base case. Each discharge pulse lasts for approximately 5 ns. The gas is initially slightly humid air, $\text{N}_2/\text{O}_2/\text{H}_2\text{O} = 79.9/20/0.1$ at 300 K and 1 atm. Before the first pulse, water is evaporated into the gap for 10 ms. The discharge is initiated by seeding a neutral plasma of 10^9 cm^{-3} near the insulator with a diameter of 100 μm . (The final values are insensitive to the density and size of this initial spot of plasma.) The discharge is then sustained by the secondary electron emission from the insulator surface, for which the emission coefficient is 0.15 for ions and 0.001 for photons. The voltage applied to the powered electrode rises to -18 kV in 0.1 ns and falls at the end of 4 ns to 0 kV in 1 ns. The interpulse period is 10 ms, during which recombination, ion-ion neutralization and diffusion extinguish the plasma. The discharge is reinitialized in the same manner for the second and third pulses. During the interpulse periods and 1 s afterglow, Poisson’s equation is not solved and quasi-neutrality is assumed, producing essentially ambipolar transport. Since the electrons that do not recombine either attach (first to O_2 in the gas phase) in less than 1 μs , or solvate in the liquid in less than 1 ns, there is little electron enhanced ambipolar transport. The diffusion is more akin to diffusion with the free diffusion coefficients of the ions. At the start of the next pulse, the charged species are forced to be absolutely neutral prior to the restart of Poisson’s equation. This is done by adjusting the densities of N_2^+ or O_2^- in the gas phase and $\text{H}_3\text{O}_{\text{aq}}^+$ and $\text{O}_{2\text{aq}}^-$ in the liquid phase. We have not included advective gas transport in the work discussed here—all transport is diffusive.

Table 2. Water reaction mechanism.

Reaction ^a	Rate coefficient ^a	Ref.
<i>Solvation reactions</i>		
$e + H_2O_{aq} \rightarrow e_{aq} + H_2O_{aq}$	2×10^9	[37] ^b
$N_2^+ + H_2O_{aq} \rightarrow N_{2aq}^+ + H_2O_{aq}$	3×10^6	b
$N_4^+ + H_2O_{aq} \rightarrow N_{4aq}^+ + H_2O_{aq}$	3×10^6	b
$O_2^+ + H_2O_{aq} \rightarrow O_{2aq}^+ + H_2O_{aq}$	3×10^6	b
$NO^+ + H_2O_{aq} \rightarrow NO_{aq}^+ + H_2O_{aq}$	3×10^6	b
$O^- + H_2O_{aq} \rightarrow O_{aq}^- + H_2O_{aq}$	3×10^6	b
$O_2^- + H_2O_{aq} \rightarrow O_{2aq}^- + H_2O_{aq}$	3×10^6	b
$H^+ + H_2O_{aq} \rightarrow H_3O_{aq}^+$	3×10^6	b
$H_3O^+ + H_2O_{aq} \rightarrow H_3O_{aq}^+ + H_2O_{aq}$	3×10^6	b
$H_5O_2^+ + H_2O_{aq} \rightarrow H_3O_{aq}^+ + H_2O_{aq} + H_2O_{aq}$	3×10^6	b
$O + H_2O_{aq} \rightarrow O_{aq} + H_2O_{aq}$	3×10^6	b
$O_3 + H_2O_{aq} \rightarrow O_{3aq} + H_2O_{aq}$	3×10^6	b
$H + H_2O_{aq} \rightarrow H_{aq} + H_2O_{aq}$	3×10^6	b
$H_2 + H_2O_{aq} \rightarrow H_{2aq} + H_2O_{aq}$	3×10^6	b
$HO_2 + H_2O_{aq} \rightarrow HO_{2aq} + H_2O_{aq}$	3×10^6	b
$OH + H_2O_{aq} \rightarrow OH_{aq} + H_2O_{aq}$	3×10^6	b
$H_2O_2 + H_2O_{aq} \rightarrow H_2O_{2aq} + H_2O_{aq}$	3×10^6	b
$NO + H_2O_{aq} \rightarrow NO_{aq} + H_2O_{aq}$	3×10^6	b
$N_xO_y + H_2O_{aq} \rightarrow N_xO_{y,aq} + H_2O_{aq}$ $N_xO_y = NO_2, NO_3, N_2O_3, N_2O_4 \text{ and } N_2O_5$	3×10^6	b
$HNO_x + H_2O_{aq} \rightarrow HNO_{x,aq} + H_2O_{aq}$ $HNO_x = HNO_2 \text{ and } HNO_3$	3×10^6	b
$HOONO + H_2O_{aq} \rightarrow HOONO_{aq} + H_2O_{aq}$	3×10^6	b
<i>In water reactions</i>		
$e_{aq} + H_2O_{aq} \rightarrow H \cdot_{aq} + OH_{aq}^-$	1.9×10^1	[36]
$e_{aq} + H_2O_{aq}^+ \rightarrow H \cdot_{aq} + OH_{aq}^-$	6×10^{11}	[36]
$e_{aq} + e_{aq} + H_2O_{aq} + H_2O_{aq} \rightarrow H_{2aq} + OH_{aq}^- + OH_{aq}^-$	$1.0 \times 10^8 M^{-3} s^{-1}$	[36]
$e_{aq} + H \cdot_{aq} + H_2O_{aq} \rightarrow H_{2aq} + OH_{aq}^-$	$2.5 \times 10^{10} M^{-2} s^{-1}$	[36]
$e_{aq} + \cdot OH_{aq} \rightarrow OH_{aq}^-$	3.0×10^{10}	[36]
$e_{aq} + \cdot O_{aq}^- + H_2O_{aq} \rightarrow OH_{aq}^- + OH_{aq}^-$	$2.2 \times 10^{10} M^{-2} s^{-1}$	[36]
$e_{aq} + H_3O_{aq}^+ \rightarrow H \cdot_{aq} + H_2O_{aq}$	2.3×10^{10}	[36]
$e_{aq} + H_2O_{2aq} \rightarrow \cdot OH_{aq} + OH_{aq}^-$	1.1×10^{10}	[36]
$e_{aq} + HO_{2aq} + H_2O_{aq} \rightarrow \cdot OH_{aq} + OH_{aq}^- + OH_{aq}^-$	$3.5 \times 10^9 M^{-2} s^{-1}$	[36]
$e_{aq} + O_{2aq} \rightarrow O_{2aq}^-$	1.9×10^{10}	[36]
$e_{aq} + O_{aq} \rightarrow O_{aq}^-$	1.9×10^{10}	[36] ^c
$H \cdot_{aq} + H_2O_{aq} \rightarrow H_{2aq} + \cdot OH_{aq}$	1×10^1	[36]
$H \cdot_{aq} + H \cdot_{aq} \rightarrow H_{2aq}$	7.5×10^9	[36]
$H \cdot_{aq} + \cdot OH_{aq} \rightarrow H_2O_{aq}$	7×10^9	[36]
$H \cdot_{aq} + OH_{aq}^- \rightarrow e_{aq} + H_2O_{aq}$	2.2×10^7	[36]
$H \cdot_{aq} + H_2O_{2aq} \rightarrow \cdot OH_{aq} + H_2O_{aq}$	9×10^7	[36]
$H_{2aq} + H_2O_{2aq} \rightarrow H \cdot_{aq} + \cdot OH_{aq} + H_2O_{aq}$	6×10^6	[36] ^c
$H \cdot_{aq} + O_{2aq} \rightarrow HO_2 \cdot_{aq}$	2.1×10^{10}	[36]
$H \cdot_{aq} + HO_2 \cdot_{aq} \rightarrow H_2O_{2aq}$	1×10^{10}	[36]
$O \cdot_{aq} + H_2O_{aq} \rightarrow \cdot OH_{aq} + \cdot OH_{aq}$	1.3×10^4	[36] ^c
$O \cdot_{aq} + O_{2aq} \rightarrow O_{3aq}$	3×10^9	[36] ^c
$\cdot OH_{aq} + \cdot OH_{aq} \rightarrow H_2O_{2aq}$	5.5×10^9	[36]
$\cdot OH_{aq} + \cdot O_{aq}^- \rightarrow HO_{2aq}^-$	2×10^{10}	[36]
$\cdot OH_{aq} + H_{2aq} \rightarrow H \cdot_{aq} + H_2O_{aq}$	4.2×10^7	[36]
$\cdot OH_{aq} + OH_{aq}^- \rightarrow \cdot O_{aq}^- + H_2O_{aq}$	1.3×10^{10}	[36]
$\cdot OH_{aq} + HO_2 \cdot_{aq} \rightarrow H_2O_{aq} + O_{2aq}$	6×10^9	[36]
$\cdot OH_{aq} + O_{2aq}^- \rightarrow OH_{aq}^- + O_{2aq}$	8×10^9	[36]
$\cdot O_{aq}^- + H_2O_{aq} \rightarrow OH_{aq}^- + \cdot OH_{aq}$	1.8×10^6	[36]
$\cdot O_{aq}^- + H_{2aq} \rightarrow OH_{aq}^- + H \cdot_{aq}$	8.0×10^7	[36]
$\cdot O_{aq}^- + H_2O_{2aq} \rightarrow O_{2aq}^- + H_2O_{aq}$	5×10^8	[36]
$\cdot O_{aq}^- + HO_{2aq} \rightarrow O_{2aq}^- + OH_{aq}^-$	4×10^8	[36]
$\cdot O_{aq}^- + O_{2aq} \rightarrow O_{3aq}^-$	3.6×10^9	[36]
$\cdot O_{aq}^- + O_{2aq}^- + H_2O_{aq} \rightarrow OH_{aq}^- + OH_{aq}^- + O_{2aq}$	$6 \times 10^8 M^{-2} s^{-1}$	[36]
$\cdot OH_{aq} + H_2O_{2aq} \rightarrow H_2O_{aq} + HO_2 \cdot_{aq}$	2.7×10^7	[36]
$\cdot OH_{aq} + HO_{2aq} \rightarrow OH_{aq}^- + HO_2 \cdot_{aq}$	7.5×10^9	[36]
$H_2O_{aq}^+ + H_2O_{aq} \rightarrow H_3O_{aq}^+ + \cdot OH_{aq}$	6×10^3	[36]

Table 2. Continued.

$\cdot\text{OH}_{\text{aq}} + \text{NO}_{2\text{aq}}^- \rightarrow \text{OH}_{\text{aq}}^- + \text{NO}_{2\text{aq}}$	1×10^{10}	[38]
$\text{H}_2\text{O}_{2\text{aq}} + \text{NO}_{2\text{aq}}^- \rightarrow \text{OONO}_{\text{aq}}^- + \text{H}_2\text{O}_{\text{aq}}$	4.5×10^8	[38]
$\text{H}\cdot_{\text{aq}} + \text{NO}_{2\text{aq}}^- \rightarrow \text{OH}_{\text{aq}}^- + \text{NO}_{\text{aq}}$	1.2×10^9	[38]
$\cdot\text{O}_{\text{aq}}^- + \text{NO}_{2\text{aq}}^- + \text{H}_2\text{O}_{\text{aq}} \rightarrow \text{OH}_{\text{aq}}^- + \text{OH}_{\text{aq}}^- + \text{NO}_{2\text{aq}}$	$3.6 \times 10^8 \text{M}^{-2} \text{s}^{-1}$	[38]
$\text{NO}_{\text{aq}} + \text{NO}_{\text{aq}} + \text{O}_{2\text{aq}} \rightarrow \text{NO}_{2\text{aq}} + \text{NO}_{2\text{aq}}$	$2.3 \times 10^6 \text{M}^{-2} \text{s}^{-1}$	[38]
$\text{NO}_{\text{aq}} + \text{NO}_{2\text{aq}} + \text{H}_2\text{O}_{\text{aq}} \rightarrow \text{HNO}_{2\text{aq}} + \text{HNO}_{2\text{aq}}$	$2 \times 10^8 \text{M}^{-2} \text{s}^{-1}$	[38]
$\text{H}\cdot_{\text{aq}} + \text{HNO}_{2\text{aq}} \rightarrow \text{NO}_{\text{aq}} + \text{H}_2\text{O}_{\text{aq}}$	4.5×10^8	[38]
$\text{NO}_{\text{aq}} + \cdot\text{OH}_{\text{aq}} \rightarrow \text{HNO}_{2\text{aq}}$	2×10^{10}	[38]
$\text{NO}_{2\text{aq}} + \text{H}\cdot_{\text{aq}} \rightarrow \text{HNO}_{2\text{aq}}$	1×10^{10}	[38]
$\text{HNO}_{3\text{aq}} + \cdot\text{OH}_{\text{aq}} \rightarrow \text{NO}_{3\text{aq}} + \text{H}_2\text{O}_{\text{aq}}$	1.2×10^8	[38]
$\text{NO}_{\text{aq}} + \text{HO}_2\cdot_{\text{aq}} \rightarrow \text{HNO}_{3\text{aq}}$	8×10^9	[38]
$\text{NO}_{2\text{aq}} + \cdot\text{OH}_{\text{aq}} \rightarrow \text{HNO}_{3\text{aq}}$	3×10^{10}	[38]
$\text{O}_{2\text{aq}}^- + \text{NO}_{\text{aq}} \rightarrow \text{NO}_{3\text{aq}}^-$	1.6×10^{10}	[38]
$\text{NO}_{\text{aq}} + \text{HO}_2\cdot_{\text{aq}} \rightarrow \text{HOONO}_{\text{aq}}$	3.2×10^9	[38]
$\text{NO}_{2\text{aq}} + \cdot\text{OH}_{\text{aq}} \rightarrow \text{HOONO}_{\text{aq}}$	1.2×10^{10}	[38]
$\text{O}_{2\text{aq}}^- + \text{NO}_{\text{aq}} \rightarrow \text{OONO}_{\text{aq}}^-$	6.6×10^9	[38]
$\text{H}_3\text{O}_{\text{aq}}^+ + \text{OH}_{\text{aq}}^- \rightarrow \cdot\text{H}_{\text{aq}} + \cdot\text{OH}_{\text{aq}} + \text{H}_2\text{O}_{\text{aq}}$	6×10^{10}	[38]
$\text{HO}_2\cdot_{\text{aq}} + \text{H}_2\text{O}_{\text{aq}} \rightarrow \text{H}_3\text{O}_{\text{aq}}^+ + \text{O}_{2\text{aq}}^-$	2×10^3	d
$\text{H}_3\text{O}_{\text{aq}}^+ + \text{O}_{2\text{aq}}^- \rightarrow \text{HO}_2\cdot_{\text{aq}} + \text{H}_2\text{O}_{\text{aq}}$	6×10^1	[39] ^d
$\text{HNO}_{2\text{aq}} + \text{H}_2\text{O}_{\text{aq}} \rightarrow \text{H}_3\text{O}_{\text{aq}}^+ + \text{NO}_{2\text{aq}}^-$	1.8×10^1	[39] ^d
$\text{H}_3\text{O}_{\text{aq}}^+ + \text{NO}_{2\text{aq}}^- \rightarrow \text{HNO}_{2\text{aq}} + \text{H}_2\text{O}_{\text{aq}}$	1.8	[39] ^d
$\text{HNO}_{3\text{aq}} + \text{H}_2\text{O}_{\text{aq}} \rightarrow \text{H}_3\text{O}_{\text{aq}}^+ + \text{NO}_{3\text{aq}}^-$	2×10^3	[39] ^d
$\text{H}_3\text{O}_{\text{aq}}^+ + \text{NO}_{3\text{aq}}^- \rightarrow \text{HNO}_{3\text{aq}} + \text{H}_2\text{O}_{\text{aq}}$	2×10^2	[39] ^d
$\text{N}_2\text{O}_{3\text{aq}} + \text{H}_2\text{O}_{\text{aq}} \rightarrow \text{HNO}_{2\text{aq}} + \text{HNO}_{2\text{aq}}$	$1.1 \times 10^4 \text{M}^{-2} \text{s}^{-1}$	[38]
$\text{N}_2\text{O}_{4\text{aq}} + \text{H}_2\text{O}_{\text{aq}} \rightarrow \text{HNO}_{2\text{aq}} + \text{HNO}_{3\text{aq}}$	$8 \times 10^2 \text{M}^{-2} \text{s}^{-1}$	[38]
$\text{N}_2\text{O}_{5\text{aq}} + \text{H}_2\text{O}_{\text{aq}} \rightarrow \text{HNO}_{3\text{aq}} + \text{HNO}_{3\text{aq}}$	$1.2 \text{M}^{-2} \text{s}^{-1}$	[38]
$\text{NO}_{2\text{aq}} + \text{NO}_{2\text{aq}} + \text{H}_2\text{O}_{\text{aq}} \rightarrow \text{HNO}_{2\text{aq}} + \text{H}_3\text{O}_{\text{aq}}^+ + \text{NO}_{3\text{aq}}^-$	$1.5 \times 10^8 \text{M}^{-2} \text{s}^{-1}$	[39]
$\text{NO}_{2\text{aq}} + \text{NO}_{2\text{aq}} + \text{H}_2\text{O}_{\text{aq}} \rightarrow \text{H}_3\text{O}_{\text{aq}}^+ + \text{NO}_{2\text{aq}}^- + \text{H}_3\text{O}_{\text{aq}}^+ + \text{NO}_{3\text{aq}}^-$	$5 \times 10^7 \text{M}^{-2} \text{s}^{-1}$	[39]
<i>Photon reactions</i>		
$h\nu + \text{H}_2\text{O}_{\text{aq}} \rightarrow \text{H}_3\text{O}_{\text{aq}}^+ + \text{e}_{\text{aq}}$	$1 \times 10^{-20} \text{cm}^2$	[40] ^c
$h\nu + \text{H}_2\text{O}_{\text{aq}} \rightarrow \text{H}\cdot_{\text{aq}} + \cdot\text{OH}_{\text{aq}}$	$1 \times 10^{-20} \text{cm}^2$	[40] ^c
<i>Reactions with hydrocarbon</i>		
$\cdot\text{OH}_{\text{aq}} + \text{RH}_{\text{aq}} \rightarrow \text{R}\cdot_{\text{aq}} + \text{H}_2\text{O}_{\text{aq}}$	2.6×10^8	[41] ^c
$\text{H}_2\text{O}_{2\text{aq}} + \text{RH}_{\text{aq}} \rightarrow \text{R}\cdot_{\text{aq}} + \cdot\text{OH}_{\text{aq}} + \text{H}_2\text{O}_{\text{aq}}$	3×10^7	[41] ^c
$\text{HO}_{2\text{aq}} + \text{RH}_{\text{aq}} \rightarrow \text{R}\cdot_{\text{aq}} + \text{H}_2\text{O}_{2\text{aq}}$	3×10^4	[41] ^c
$\text{O}\cdot_{\text{aq}} + \text{RH}_{\text{aq}} \rightarrow \text{R}\cdot_{\text{aq}} + \cdot\text{OH}_{\text{aq}}$	6×10^6	[42] ^c
$\text{O}_{3\text{aq}} + \text{RH}_{\text{aq}} \rightarrow \text{R}\cdot_{\text{aq}} + \cdot\text{OH}_{\text{aq}} + \text{O}_{2\text{aq}}$	5×10^5	[42] ^c
$\text{H}\cdot_{\text{aq}} + \text{RH}_{\text{aq}} \rightarrow \text{R}\cdot_{\text{aq}} + \text{H}_{2\text{aq}}$	5×10^5	[41] ^c

^a Aqueous species have an 'aq' subscript. Rate coefficients have units of $\text{M}^{-1} \text{s}^{-1}$ ($\text{l mole}^{-1} \text{s}^{-1}$) unless noted otherwise. ' \cdot ' represents a free radical.

^b The solvation rate coefficient was estimated to be faster than other liquid reactions in order to not be rate limiting.

^c Approximated by analogy.

^d The rate coefficient is estimated according to the thermodynamic hydrolysis in liquid water.

In work to be reported elsewhere, a wind of only tens of cm s^{-1} is sufficient to affect the plasma–water interaction.

We have assumed that the underlying tissue consumes the radical species produced in the liquid, and so acts as a sink for these species. We have not addressed the change in the biochemistry of the tissue resulting from those reactions as being beyond the scope of this study. It is this consumption of radicals by the tissue that in part is responsible for the dependence of radical fluences to the tissue on the thickness of the liquid layer.

3. DBD plasma filaments incident onto water

The time evolution of a typical DBD filament incident onto the water surface is shown in figure 2, where the gas phase

electron density, n_e , electron temperature, T_e , E/N (electric field/gas number density) and electron impact ionization source, S_e , are shown. The discharge starts at the top electrode where the cloud of initial plasma is seeded. The density of the seed electrons was optimized to be 10^9cm^{-3} with 0.1 mm diameter, which does not affect the discharge properties. The lower limit of seed electrons to initiate the discharge is 10^8cm^{-3} . Upon application of the -18 kV pulse, the electrons avalanche downwards, at first in a Townsend-like mode, and then in a streamer-like mode, and reach the liquid layer in 1.7 ns with density of 10^{13}cm^{-3} . At this time, E/N is fairly uniform in the gap, around 100 Td ($1 \text{ Td} = 10^{-17} \text{ V cm}^2$). T_e is about 4 eV and the ionization source is $10^{22} \text{cm}^{-3} \text{s}^{-1}$. Once the discharge reaches and begins to charge the liquid layer, a backward streamer develops and finally reaches the

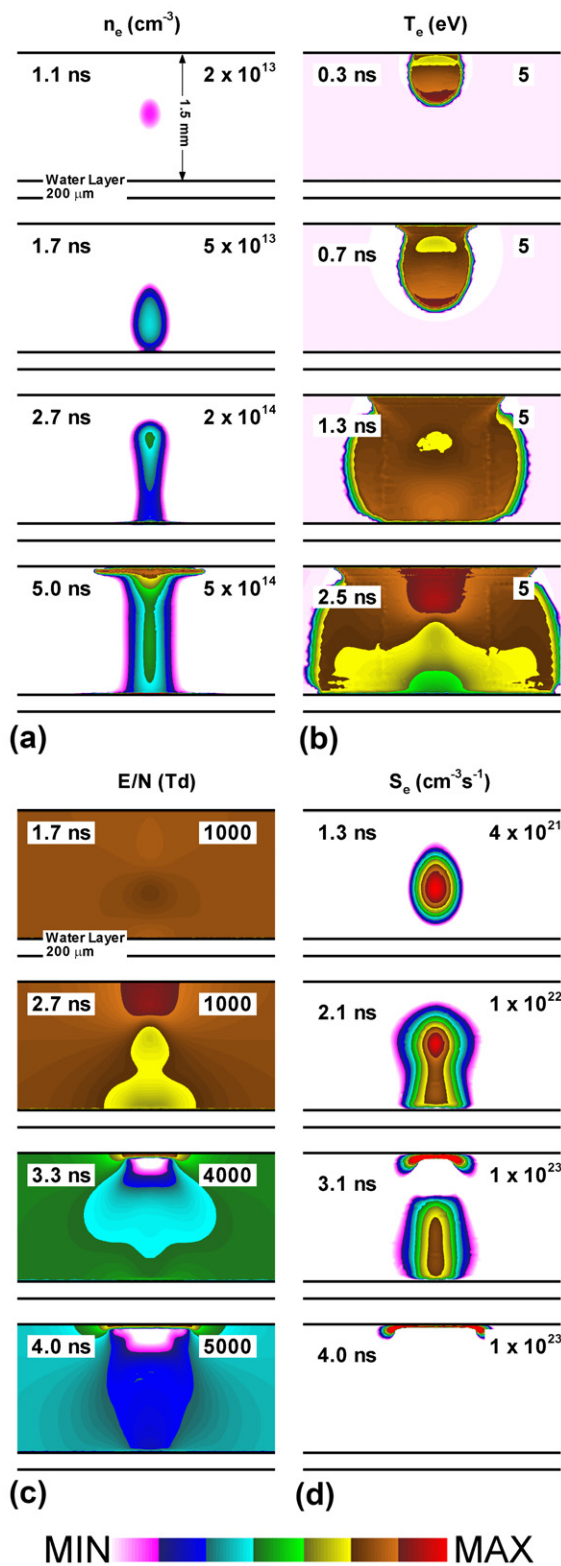


Figure 2. Time evolution of (a) electron density, n_e , (b) electron temperature, T_e , (c) E/N (electric field/gas number density) and (d) electron impact ionization source, S_e , for a negative discharge operated at -18 kV for 5 ns over a $200 \mu\text{m}$ water layer. The gas gap and water layer are shown. The initial gas is 1 atm, $N_2/O_2/H_2O = 79.9/20/0.1$, and water evaporates from the surface. The contours for n_e and S_e are plotted on a log scale over three decades, and for E/N over two decades. Maximum values are shown in each frame.

top insulator at 2.7 ns. At that point, a conductive channel forms and the electron density increases to $2 \times 10^{14} \text{ cm}^{-3}$. A sheath begins to form at the dielectric surface, the E/N near the insulator reaches 1000 Td and T_e increases to 8 eV. The ionization source, $10^{23} \text{ cm}^{-3} \text{ s}^{-1}$, is then confined to a thin surface layer which spreads along the dielectric. Once bridging the gap, the discharge spreads over the surface of the insulator and the water layer, as wide as 1 mm. The spread is wider on the insulator since its capacitance is smaller.

Considering the negative polarity of the pulse, positive ions striking the insulator surface produce secondary electrons to maintain the streamer while the surface of the dielectric charges. As a result, the electron density near the top insulator is as high as $5 \times 10^{14} \text{ cm}^{-3}$. On the other hand, the water layer is to some degree a sink where electrons strike and quickly become solvated. As a result, the electron density is lower, 10^{13} cm^{-3} , at the surface of the water.

The air is initially slightly humid, having 0.1% H_2O ($2.5 \times 10^{16} \text{ cm}^{-3}$), and is humidified as water evaporates into the gap. The water vapour density across the gap at the time the voltage is applied is shown in figure 3(a). The density of the H_2O is $5 \times 10^{17} \text{ cm}^{-3}$ at the water surface, as given by the room temperature vapour pressure of the water, 27 Torr [35]. At the top of the gap, the density of the H_2O is $7 \times 10^{16} \text{ cm}^{-3}$. The densities of plasma-produced H_2O^+ and OH are shown in figure 3(b), with and without evaporation. In the absence of evaporation, the maximum density of gas phase H_2O^+ and OH above the water are 3.1×10^{11} and $1.1 \times 10^{12} \text{ cm}^{-3}$. With evaporation, the densities are 1.5×10^{12} and $1.2 \times 10^{13} \text{ cm}^{-3}$. The saturated water vapour above the liquid significantly increases the densities of ROS in close vicinity to the water surface. We provide this comparison to emphasize the sensitivity of the results discussed below to the environmental conditions. For example, how long the DBD source is positioned above the water layer, a few degree change in water temperature (thereby affecting the vapour pressure), and cross-currents of air blowing across the liquid are all capable of changing the humidity within the gas, so affecting the final outcome of ROS production.

The general sequence of reactions we will discuss below are summarized here. The notation typically used for liquid phase reactions expresses second-order rate coefficients with units of $(\text{mole/l})^{-1} \text{ s}^{-1}$ or $\text{M}^{-1} \text{ s}^{-1}$. A gas kinetic rate coefficient refers to a reaction that has no activation barrier nor steric hindrance, and so reactions occur with every collision. For atoms and molecules with moderate molecular weights at room temperature, a gas kinetic rate coefficient is about $10^{-10} \text{ cm}^3 \text{ s}^{-1}$. So the equivalent gas kinetic (EGK) rate coefficient in the liquid phase is about $6 \times 10^{10} \text{ M}^{-1} \text{ s}^{-1}$. We call these reactions EGK. Reactions with liquid water with an EGK rate coefficient occur in a few ps.

Positive ions. The ionization potential of water is 12.6 eV, which is smaller than all of the major ions produced in the streamer (N_2^+ , N_4^+ , O_2^+). When striking the water surface, the major ions charge exchange with H_2O_{aq} to form $H_2O_{\text{aq}}^+$. The rate coefficient is likely near EGK and so, given the water density of $3 \times 10^{22} \text{ cm}^{-3}$, this reaction likely occurs in tens

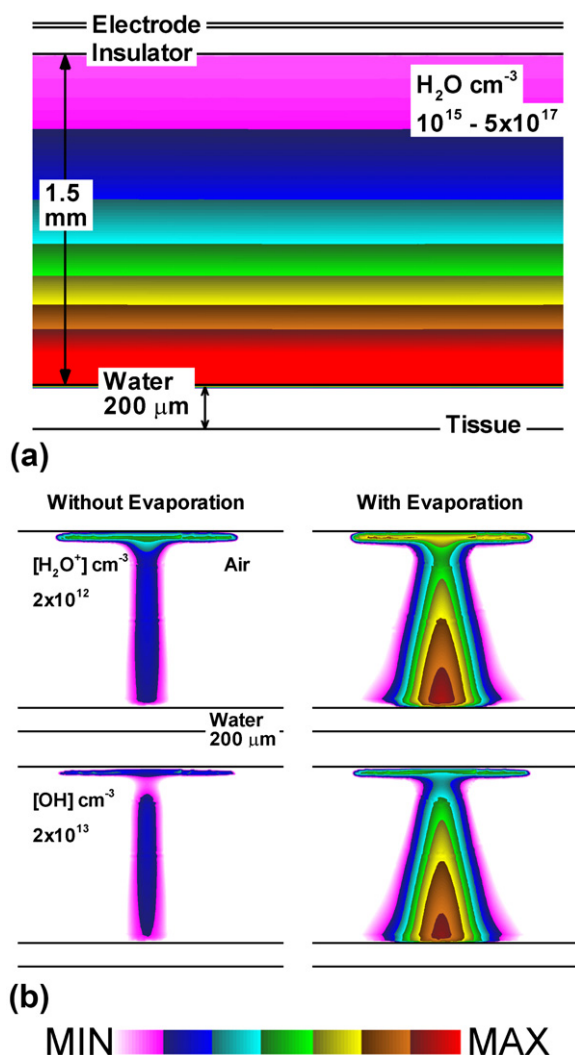


Figure 3. Properties due to water evaporation. (a) The density of water vapour in the gap for 10 ms evaporation. The density of the saturated water vapour at the water surface is about 3% of the ambient gases at 300 K. (b) The densities of H_2O^+ and OH in the discharge with and without evaporation. The initial gas mixture is 1 atm, $\text{N}_2/\text{O}_2/\text{H}_2\text{O} = 79.9/20/0.1$. Contours for H_2O^+ and OH are plotted on a log scale over three decades with the maximum density shown in each frame.

of ps to perhaps 1 ns at most. $\text{H}_2\text{O}_{\text{aq}}^+$ then charge exchanges with $\text{H}_2\text{O}_{\text{aq}}$ to form $\text{H}_3\text{O}_{\text{aq}}^+$ and OH_{aq} . With a rate coefficient of $6 \times 10^3 \text{M}^{-1} \text{s}^{-1}$, this charge exchange occurs in a few μs .

Electrons. Electrons striking the water solvate to form e_{aq} within a few ps. e_{aq} is an electron surrounded by water molecules, and can be thought of as a low mobility and somewhat low reactivity electron. Here the purity of the water is important. The e_{aq} slowly reacts with the $\text{H}_2\text{O}_{\text{aq}}$ to form H_{aq} and OH_{aq}^- , with reaction times of a few ms. The e_{aq} will attach to $\text{O}_{2\text{aq}}$ to form $\text{O}_{2\text{aq}}^-$ with a rate coefficient $2 \times 10^{10} \text{M}^{-1} \text{s}^{-1}$, nearly EGK. It is common for water to have dissolved $\text{O}_{2\text{aq}}$, in our case $\text{O}_{2\text{aq}} = 8 \text{ppm}$ or $4 \times 10^{-4} \text{M}$, which produces attachment times of about 100 ns. Similar attachment or dissociative attachment reactions with EGK rate

coefficients occur with (reaction products are in parenthesis) $\text{H}_2\text{O}_{2\text{aq}}$ ($\text{OH}_{\text{aq}} + \text{OH}_{\text{aq}}^-$), OH_{aq} (OH_{aq}^-) and O_{aq} (O_{aq}^-).

Negative ions. We have assumed that negative ions entering the liquid from the gas phase will solvate as their equivalent aqueous forms. The major negative ions in the gas phase are O_2^- and O^- . When reaching the water, O_2^- is solvated to $\text{O}_{2\text{aq}}^-$ in a few ps, which is one of the dominant negative ions in the liquid. As mentioned above, electron attachment to produce $\text{O}_{2\text{aq}}^-$ is fast—microseconds—and produces more $\text{O}_{2\text{aq}}^-$ than the solvation of the gas phase negative ion. Another source of $\text{O}_{2\text{aq}}^-$ comes from the hydrolysis of $\text{HO}_{2\text{aq}}$, which is produced by H_{aq} combining with $\text{O}_{2\text{aq}}$. This process is slow, occurring in a few ms, and depends strongly on the production of H_{aq} in the water. Once formed, $\text{O}_{2\text{aq}}^-$ reacts with dissolved NO_{aq} with a rate coefficient of $3.6 \times 10^9 \text{M}^{-1} \text{s}^{-1}$, or charge exchanges with OH_{aq} to form OH_{aq}^- with a rate coefficient of $6 \times 10^9 \text{M}^{-1} \text{s}^{-1}$. The relative branchings for these reactions depend on the densities of NO_{aq} and OH_{aq} . OH_{aq} is produced in the water during the current pulse by the photodissociation of water, while NO_{aq} is produced by the solvation of gas phase NO during the afterglow. As a result, the $\text{O}_{2\text{aq}}^-$ charge exchange with OH_{aq} occurs earlier than the reaction with NO_{aq} . O^- , as well as its solvated counterpart, O_{aq}^- , is highly reactive. O_{aq}^- reacts with e_{aq} to dissociate $\text{H}_2\text{O}_{\text{aq}}$ to form OH_{aq}^- with a rate coefficient $2.2 \times 10^{10} \text{M}^{-2} \text{s}^{-1}$; or neutralizes $\text{H}_3\text{O}_{\text{aq}}^+$ to form OH_{aq} with a rate coefficient $2.3 \times 10^{10} \text{M}^{-1} \text{s}^{-1}$. Both reactions are nearly EGK. The density of O_{aq}^- diminishes in a microsecond or less after the discharge pulse. Since the maximum density of O_{aq}^- is only 10^{12}cm^{-3} in water and the $\text{H}_3\text{O}_{\text{aq}}^+$ density does not rise before the density of O_{aq}^- diminishes, these reactions do not significantly affect the liquid chemistry.

ROS. The most important ROS in water for these conditions are OH_{aq} , $\text{H}_2\text{O}_{2\text{aq}}$ and $\text{O}_{3\text{aq}}$. OH_{aq} can be produced directly in water or through the solvation of gas phase OH. OH_{aq} is produced in the water by photolysis, electron impact dissociation at the surface (though this is not important for these conditions), charge exchange of $\text{H}_2\text{O}_{\text{aq}}^+$ with water and ion–ion recombination. These reactions occur in short times—from sub-microsecond for photolysis, to tens of microseconds for ion–ion recombination. In the afterglow, gas phase OH solvates in milliseconds as the OH diffuses into the water with a large Henry's law constant, 6.92×10^2 . $\text{H}_2\text{O}_{2\text{aq}}$ is produced in a few ms by the mutual reaction of OH_{aq} with a rate coefficient of $5.5 \times 10^9 \text{M} \text{s}^{-1}$, about 0.1 EGK. In the afterglow, gas phase H_2O_2 also solvates into the water with a large Henry's law constant, 1.92×10^6 , which also contributes to the density of $\text{H}_2\text{O}_{2\text{aq}}$. $\text{O}_{3\text{aq}}$ is not directly produced in the water since the density of O_{aq} is small. In the gas phase, O is produced through the electron impact dissociation of O_2 and dissociative excitation transfer from $\text{N}_2(\text{A})$ but quickly combines with O_2 to form O_3 . So little O survives to diffuse into the water, while dissociation of $\text{O}_{2\text{aq}}$ is difficult. Solvation of gas phase O_3 dominates the production of $\text{O}_{3\text{aq}}$. Although O_3 has a small Henry's law constant, 0.3 (much smaller than for OH

and H_2O_2), its large density, as high as 10^{15} cm^{-3} after a few pulses, still produces a high aqueous density of $\text{O}_{3\text{aq}}$, averaging $5 \times 10^{14} \text{ cm}^{-3}$.

RNS. The dominant RNS in water for our conditions are $\text{HNO}_{2\text{aq}}$, $\text{HNO}_{3\text{aq}}$ and HOONO_{aq} , and their conjugate ions, $\text{NO}_{2\text{aq}}^-$, $\text{NO}_{3\text{aq}}^-$ and $\text{ONOO}_{\text{aq}}^-$. The RNS can be formed in both the gas and liquid phase, and the formation channels are similar. The aqueous RNS originate as N_xO_y (NO , NO_2 , NO_3 , N_2O_3 , N_2O_4 , N_2O_5), which is mainly formed in the gas phase during the afterglow a few milliseconds after the discharge pulse. Of the N_xO_y , NO dominates with a maximum density of 10^{14} cm^{-3} , followed by NO_2 with a density of 10^{12} cm^{-3} for the few discharge pulses we simulated. Other nitrogen species have densities below 10^{11} cm^{-3} . HNO_2 , either in gas phase or in the liquid, is produced by three-body reactions, for example, $\text{NO} + \text{OH} + M$, with a rate coefficient of $6 \times 10^{-31} \text{ cm}^6 \text{ s}^{-1}$ in gas phase or $2 \times 10^{10} \text{ M}^{-1} \text{ s}^{-1}$ in the liquid. NO and NO_2 have small Henry's law coefficients, 0.044 and 0.28, respectively. The solvation processes of NO and NO_2 are therefore slow enough that HNO_2 has sufficient time to be formed in the gas phase. On the other hand, HNO_2 has a large Henry's law constant, 1.15×10^3 , which allows gas phase HNO_2 to rapidly solvate. Therefore, the solvation process plays a significant role, 40%, in aqueous $\text{HNO}_{2\text{aq}}$ production.

HNO_3 forms through similar channels to HNO_2 . HNO_3 is formed, either in the gas phase or in the liquid, by $\text{NO} + \text{HO}_2 + M$ with a rate coefficient of $2 \times 10^{-30} \text{ cm}^6 \text{ s}^{-1}$ in the gas phase or $8 \times 10^9 \text{ M}^{-1} \text{ s}^{-1}$ in the liquid; and by $\text{OH} + \text{NO}_2 + M$ with a rate coefficient of $1.7 \times 10^{-30} \text{ cm}^6 \text{ s}^{-1}$ in the gas phase or $3 \times 10^{10} \text{ M}^{-1} \text{ s}^{-1}$ in the liquid. In the gas phase, the density of NO_2 is lower than that of NO by a factor of nearly 100 after three pulses, and the density of HO_2 is even lower, $\approx 10^9 \text{ cm}^{-3}$. As a result, the latter reaction is more important in forming HNO_3 , and the density of HNO_3 (10^{11} cm^{-3}) is much smaller than that of HNO_2 (10^{12} cm^{-3}) for the number of discharge pulses we simulated. However, HNO_3 has a larger Henry's law constant (4.8×10^6) than HNO_2 (1.15×10^6). The end result is that the solvation of HNO_3 from the gas phase contributes 11% of the $\text{HNO}_{3\text{aq}}$.

HOONO , an isomer of HNO_3 , forms through similar channels. HOONO has a linear molecular structure and higher oxidizing energy. [43] HOONO is produced, either in the gas phase or in the liquid, by reactions of $\text{NO} + \text{HO}_2$, with a rate coefficient of $2.31 \times 10^{-13} \text{ cm}^3 \text{ s}^{-1}$ in the gas phase or $3.2 \times 10^9 \text{ M}^{-1} \text{ s}^{-1}$ in the liquid; and by reactions of $\text{NO}_2 + \text{OH}$, with a rate coefficient of $1.57 \times 10^{-11} \text{ cm}^3 \text{ s}^{-1}$ in the gas phase or $1.2 \times 10^{10} \text{ M}^{-1} \text{ s}^{-1}$ in the liquid. Similar to HNO_3 production, the latter reaction is more prominent. The ratio of HOONO to HNO_3 in the gas phase is about 40% in our model. The Henry's law constant of HOONO is basically the same as for HNO_3 , and so its solvation is rapid. The conjugate ions of these acids come from their hydrolysis. $\text{HNO}_{2\text{aq}}$ is a weak acid and about 1% of $\text{HNO}_{2\text{aq}}$ hydrolyses in water, and so the density of $\text{NO}_{2\text{aq}}^-$ is only about 10^{11} cm^{-3} . $\text{HNO}_{3\text{aq}}$ and HOONO_{aq} are stronger acids and essentially completely hydrolyse in water, resulting in the density of $\text{NO}_{3\text{aq}}^-$ and $\text{ONOO}_{\text{aq}}^-$ being 10^{13} cm^{-3} .

Photons. The threshold energy for the photo-dissociation of $\text{H}_2\text{O}_{\text{aq}}$ is 7.6 eV and that for photo-ionization is 12.6 eV, both of which are lower in energy than the VUV photons expected to be produced by the electron avalanche onto the surface of the water. The cross-section for both of these processes is $1 \times 10^{-20} \text{ cm}^2$, which yields a mean free path for the absorption of VUV photons in the water of about $30 \mu\text{m}$.

The sum of the electron and negative ion densities, and the positive ion densities, are shown in figure 4 in the gas phase and in the liquid. The gas phase densities are shown at the end of the voltage pulse. The enlargements of densities in the liquid are at times during the pulse, in the interpulse afterglow and during the terminal afterglow following the third pulse. (Recall that the discharge pulses begin at $t = 0 \text{ s}$, 10 ms and 20 ms, and the last afterglow extends to 1 s.) For the negative species, the densities of e_{aq} and the sum of $\text{NO}_{3\text{aq}}^-$ and $\text{O}_{2\text{aq}}^-$ are shown. For the positive species, $\text{H}_2\text{O}_{\text{aq}}^+$ and $\text{H}_3\text{O}_{\text{aq}}^+$ are shown. As a negative discharge, electrons in the gas phase are accelerated by the applied electric field into the surface of the water where they essentially immediately solvate to form e_{aq} . Since the mobility of e_{aq} is smaller by a factor of at least 10^4 than in the gas phase due to the higher density of collision partners and larger effective mass, there is net negative charging of the surface of the water similar to the surface of the dielectric in a DBD. On the first discharge pulse, there are few other species in the water other than dissolved oxygen, $\text{O}_{2\text{aq}}$. As a result, during the first early afterglow e_{aq} primarily attaches to $\text{O}_{2\text{aq}}$ to form $\text{O}_{2\text{aq}}^-$. This attachment occurs within a few μs . During the discharge pulse, the photo-dissociation of $\text{H}_2\text{O}_{\text{aq}}$ generates OH_{aq} , which provides another prompt partner for attachment. The dissociative attachment to $\text{H}_2\text{O}_{\text{aq}}$ to form H_{aq} and OH_{aq}^- occurs in significant numbers only in the terminal afterglow.

During the interpulse and terminal afterglows, NO_x from the gas phase diffuses into the water, which then opens channels for other attachment processes. The diffusion of NO into the liquid enables a charge exchange between NO_{aq} and $\text{O}_{2\text{aq}}^-$ to form $\text{NO}_{3\text{aq}}^-$. The sequence of events that occurs during and after each discharge pulse is the drift of gas phase electrons into the liquid, rapid solvation to form e_{aq} , followed by two charge exchanges to form $\text{O}_{2\text{aq}}^-$ and $\text{NO}_{3\text{aq}}^-$. The rate of the second charge exchange reaction increases as the fluence of NO_x from the gas phase into the water increases with each successive discharge pulse. The rate of the first charge exchange depends on the density of dissolved $\text{O}_{2\text{aq}}$. Since the dissolved $\text{O}_{2\text{aq}}$ is a function of water temperature, we expect that the rate at which these initiating attachment processes occur will also be temperature dependent. During later discharge pulses and during the terminal afterglow, nitric acid, HNO_3 is formed in the gas phase and diffuses into the water. $\text{NO}_{3\text{aq}}^-$ is then also generated by the hydrolysis of $\text{HNO}_{3\text{aq}}$, which also produces hydronium, $\text{H}_3\text{O}_{\text{aq}}^+$. During the terminal afterglow, the end products of the hydrolysis and charge exchange result in $\text{O}_{2\text{aq}}^-$ and $\text{NO}_{3\text{aq}}^-$ being the dominant negative ions. These ions diffuse through the $200 \mu\text{m}$ water later to reach the underlying tissue. At the end of the 1 s afterglow, the combined densities of $\text{O}_{2\text{aq}}^-$ and $\text{NO}_{3\text{aq}}^-$ above the tissue are $2.5 \times 10^{13} \text{ cm}^{-3}$, or a molar density of $4.2 \times 10^{-8} \text{ M}$. Recall that this density results from three discharge pulses.

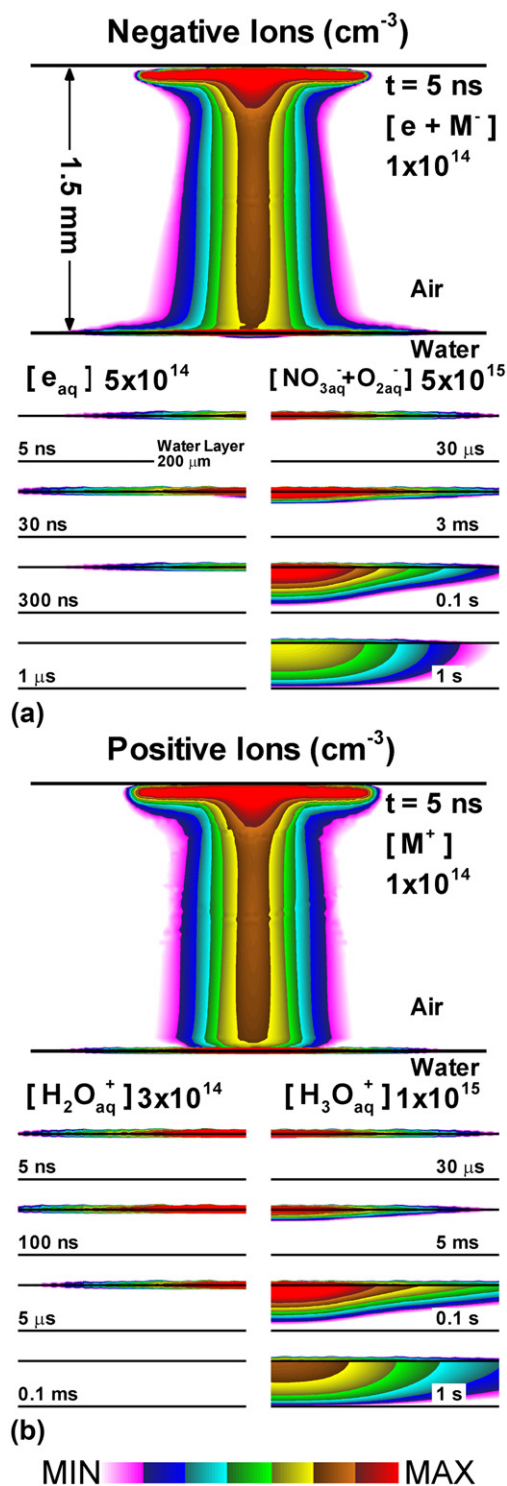


Figure 4. Ion densities in the gas gap and in the liquid layer. In the top of each frame is the density in the gas phase at the end of the first discharge pulse. In the bottom of each frame are time histories of ions in the $200 \mu\text{m}$ water layer a times during the three discharge pulses, interpulse afterglow and terminal afterglow. (‘_{aq}’ represents an aqueous species.) (a) Electrons and negative ions in the gas gap, and solvated $\text{O}_{2\text{aq}}^-$ and $\text{NO}_{3\text{aq}}^-$ in the liquid. Electrons dominate the negatively charged species in the gas gap. $\text{O}_{2\text{aq}}^-$ and $\text{NO}_{3\text{aq}}^-$ dominate the negative ions in the liquid. (b) Positive ions in the gas gap, and $\text{H}_2\text{O}_{\text{aq}}^+$ and $\text{H}_3\text{O}_{\text{aq}}^+$ in the liquid. O_2^+ and H_2O^+ dominate the positive ions in the gas gap and $\text{H}_3\text{O}_{\text{aq}}^+$ dominates the positive ions in the liquid. The contours are plotted on a 3-decade log-scale with the maximum values noted in each frame.

The sum of the positive ions is shown in figure 4(b). In the gas phase just above the water at the end of the voltage pulse, the dominant positive ions are N_2^+ ($6.6 \times 10^9 \text{ cm}^{-3}$), N_4^+ ($4.1 \times 10^{11} \text{ cm}^{-3}$), O_2^+ ($1.1 \times 10^{13} \text{ cm}^{-3}$) and H_2O^+ ($6.1 \times 10^{11} \text{ cm}^{-3}$). O_2^+ dominates the positive ions since it has the lower ionization potential. The density of H_2O^+ is second to O_2^+ and exceeds that of N_4^+ due to the high water vapour concentration at the surface of the water. Due to this being a negative discharge, the net drift of positive ions is towards the top insulator, and so during the discharge pulse, the fluence of positive ions into the water is smaller than for electrons. N_2^+ and O_2^+ solvate and quickly charge exchange to form $\text{H}_2\text{O}_{\text{aq}}^+$, whereas H_2O^+ directly solvates to form $\text{H}_2\text{O}_{\text{aq}}^+$. The production of $\text{H}_2\text{O}_{\text{aq}}^+$ is significantly enhanced by photoionization. Photoionization contributes 62% to the initial production of $\text{H}_2\text{O}_{\text{aq}}^+$, a process that is enabled by the plasma touching the water and so allowing the plasma generated VUV to reach the surface of the water. An equal rate of photodissociation occurs, which is an important source of OH_{aq} and H_{aq} . In the absence of H diffusing from the gas phase into the water, there are few ways to produce H_{aq} outside of photodissociation. These photolysis reactions producing $\text{H}_2\text{O}_{\text{aq}}^+$, OH_{aq} and H_{aq} may be a distinguishing feature between the remote and direct plasma exposure of water.

$\text{H}_2\text{O}_{\text{aq}}^+$ penetrates only a few micrometres into the water before forming hydronium $\text{H}_3\text{O}_{\text{aq}}^+$, a reaction that also produces OH_{aq} . Direct charge exchange and photoionization are the dominant sources of $\text{H}_3\text{O}_{\text{aq}}^+$ prior to the terminal afterglow. During the terminal afterglow, $\text{H}_3\text{O}_{\text{aq}}^+$ is also formed from the hydrolysis of neutral hydroperoxyl radicals ($\text{HO}_{2\text{aq}}$), nitrous acid ($\text{HNO}_{2\text{aq}}$) and nitric acid ($\text{HNO}_{3\text{aq}}$). The majority of $\text{H}_3\text{O}_{\text{aq}}^+$ is ultimately produced by these hydrolysis reactions during the afterglow. $\text{H}_3\text{O}_{\text{aq}}^+$ is produced dominantly by $\text{HNO}_{3\text{aq}}$ hydrolysis, while in the absence of nitrogen species $\text{HO}_{2\text{aq}}$ could be the dominant source providing $\text{H}_3\text{O}_{\text{aq}}^+$. $\text{H}_3\text{O}_{\text{aq}}^+$ is the terminal positive ion, which drifts through the water layer to the underlying tissue. At the end of the terminal 1 s afterglow, the density of $\text{H}_3\text{O}_{\text{aq}}^+$ above the tissue is $2.3 \times 10^{14} \text{ cm}^{-3}$, or a molar density of $3.8 \times 10^{-7} \text{ M}$. The persistence of $\text{H}_3\text{O}_{\text{aq}}^+$ has been experimentally observed to last for as long as days [23].

$\text{H}_3\text{O}_{\text{aq}}^+$ is responsible for the acidification of the water and the lowering of its pH value. Experimentally, the pH of distilled water has been reduced to as low as 4 after 3 min of plasma treatment [25]. For the results discussed here, in which we have simulated only three pulses, the local maximum density of $\text{H}_3\text{O}_{\text{aq}}^+$ is $3 \times 10^{15} \text{ cm}^{-3}$ (or $5 \times 10^{-6} \text{ M}$) producing a local pH value of 5.3, and an average pH value of about 6, so the water is only weakly acidified. More pulses will produce a lower pH value and a more acidic solution. For example, after simulating six pulses, the maximum density of $\text{H}_3\text{O}_{\text{aq}}^+$ is $5 \times 10^{15} \text{ cm}^{-3}$ (or $8 \times 10^{-6} \text{ M}$), producing a local pH value of 5.1 and an average pH value of about 5.8. Since $\text{H}_3\text{O}_{\text{aq}}^+$ to some degree accumulates on a pulse-to-pulse basis, it is not unexpected to produce small pH values after many pulses.

Experimental investigations have suggested that bacteria killing species in water include hydroxyl radicals [27], hydrogen-peroxide and ozone [28], collectively known as

ROS; and RNS in the form of nitric acid [25, 27] and peroxyntirite [29]. Unlike gas phase charged species, which largely recombine or neutralize prior to diffusing to the surface of the liquid, the lifetimes of neutral radicals are long enough that these plasma produced species are able to diffuse into the water without significant losses. Species such as O_3 and N_xO_y that accumulate in the gas phase pulse-to-pulse represent a large reservoir of reactivity, which eventually diffuses into the liquid. This reactivity is enhanced by Henry's law constants larger than 1.0 for most neutral radicals except NO , NO_2 and O_3 . This means that the water is able to quickly solvate the neutral radicals resulting in the water layer absorbing more neutral radicals than charged species.

One of the possible interactions of ROS with cell membranes is the peroxidation of the membrane lipids. OH_{aq} and H_2O_{2aq} are highly reactive radicals, with oxidizing potentials of 2.8 eV and 1.78 eV, respectively. A synergistic effect in bacteria killing involving OH_{aq} and H_2O_{2aq} can become even stronger in low pH environments [25, 28]. The densities of OH and H_2O_2 in the gas phase from the end of the current pulse to 3 ms are shown in figure 5. The densities of OH_{aq} and H_2O_{2aq} at times from the end of the current pulse to the end of the terminal afterglow are also shown. The OH in the gas phase is dominantly produced by the electron impact dissociation of water vapour and so its density is largest near the surface of the liquid where the water vapour density is the highest. The density of OH is also high near the top insulator because the electron density and temperature are high there. OH is depleted by diffusion into the water or formation of H_2O_2 . The maximum density of OH at the end of the current pulse (5 ns) is $1.3 \times 10^{13} \text{ cm}^{-3}$. By 3 ms, the density of OH has decreased to $9.1 \times 10^{11} \text{ cm}^{-3}$. During the interpulse afterglow, the majority of OH has been depleted and the H_2O_2 density is $3.3 \times 10^{11} \text{ cm}^{-3}$. H_2O_2 continues to accumulate pulse-to-pulse, from $3.3 \times 10^{11} \text{ cm}^{-3}$ at 3 ms to $1.6 \times 10^{12} \text{ cm}^{-3}$ at 23 ms. H_2O_2 has a larger Henry's law constant than OH and therefore more rapidly solvates into the water.

In addition to diffusion and solvation processes, OH_{aq} is also produced by photodissociation at the surface of the water by VUV produced by the plasma, and by the formation of $H_3O_{aq}^+$ by charge exchange with $H_2O_{aq}^+$. Through this charge exchange process, every positive ion incident onto the water produces at least one OH_{aq} . In spite of its short duration, a large photon flux onto the surface of the water still results in a significant production of OH_{aq} . For example, integrated over the three pulses simulated here, the proportion of OH_{aq} initially produced by photodissociation is 39%, by charge exchange is 27%, and by solvation of OH is only 3%. The timings of these contributions is quite different. Photodissociation and charge exchange occur nearly coincident with the discharge pulse whereas diffusion occurs throughout the afterglow.

The mean free path for charge exchange and photodissociation in the water is at best 20–30 μm , so the majority of the OH_{aq} is produced at the top of the liquid, which is also the entry point for OH diffusing from the gas phase. The maximum density of OH_{aq} at the top of the water layer is $1.6 \times 10^{15} \text{ cm}^{-3}$ (or $2.6 \times 10^{-6} \text{ M}$) at 10 μs after the discharge pulse. Since the diffusion through the water layer is slow,

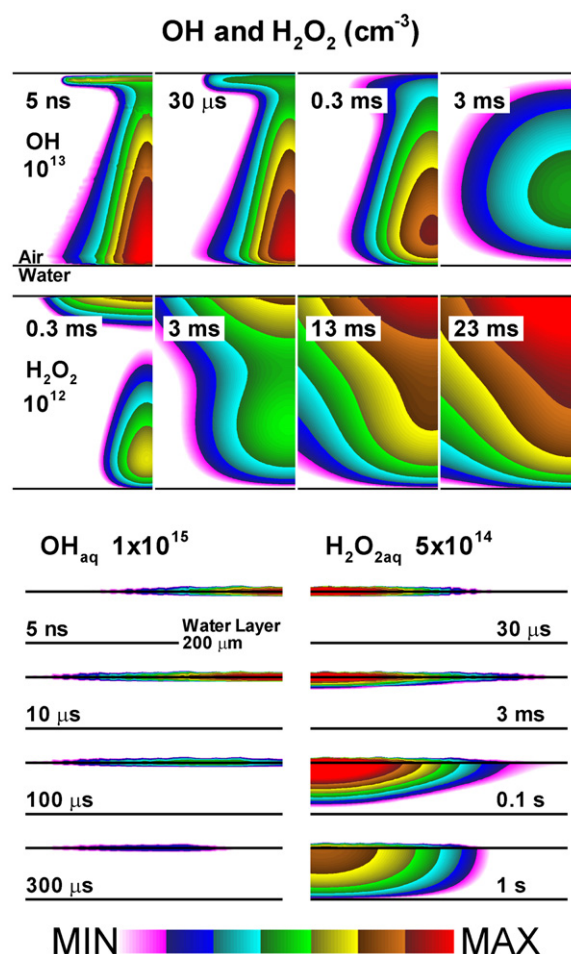


Figure 5. The time evolution of OH and H_2O_2 densities in the (top) gas gap and (bottom) 200 μm water layer. The densities of OH and OH_{aq} are shown during the first pulse and interpulse afterglow. H_2O_2 and H_2O_{2aq} densities are shown accumulating after each pulse (0, 10 ms, 20 ms) and during the terminal afterglow. The contours are plotted on a 3-decade log-scale with the maximum values noted in each frame.

the majority of OH_{aq} mutually reacts to form H_2O_{2aq} before OH_{aq} can reach the underlying tissue for a 200 μm thick water layer. H_2O_{2aq} has a lower oxidizing potential than OH_{aq} , but it is nevertheless an efficient agent to transport the oxidizing power originally generated by electron impact processes in the gas phase through the water. In the absence of hydrocarbon species, H_2O_{2aq} is the terminal species in this reaction chain, which then diffuses through the water layer to reach the underlying tissue. The maximum density of H_2O_{2aq} near the surface is $1.5 \times 10^{15} \text{ cm}^{-3}$ (or $2.5 \times 10^{-6} \text{ M}$). At the end of the terminal afterglow, the density of H_2O_{2aq} at the tissue is $5.5 \times 10^{13} \text{ cm}^{-3}$ (or $9.2 \times 10^{-8} \text{ M}$). In our mechanism, H_2O_2 reacts with the tissue and so the fluence to the tissue (the integrated flux) is perhaps the better measure of reactivity. Fluences are discussed below.

Although H_2O_{2aq} is fairly stable in water in the absence of hydrocarbon in our model, H_2O_{2aq} can be photolysed to OH by UV fluxes (250–300 nm) [44] or can dissociate in the presence of ferrous ions, Fe_{aq}^{2+} [45]. Although not included in our mechanism, we do not expect the photolysis of H_2O_{2aq} to be

significant. The photons are produced by the short discharge and active afterglow which terminates before large amounts of $\text{H}_2\text{O}_{2\text{aq}}$ are formed. However, it may be that in a pulse-periodic steady state, the photolysis of $\text{H}_2\text{O}_{2\text{aq}}$ is important. In the $\text{H}_2\text{O}_{2\text{aq}}$ decomposition by $\text{Fe}_{\text{aq}}^{2+}$ (the Fenton reaction), OH_{aq} and OH_{aq}^- are produced, and the ferrous ion becomes a ferric ion, $\text{Fe}_{\text{aq}}^{3+}$. In our mechanism we have not included ferrous or ferric ions, however, blood and blood serum do contain ferrous ions which are responsible for the transport of oxygen [16]. In the case of treating blood or blood serum in a wound, it is possible that $\text{H}_2\text{O}_{2\text{aq}}$ diffuses deeply into the liquid layer where it subsequently dissociates into OH_{aq} by reacting with ferrous ions. The relative proportion of $\text{Fe}_{\text{aq}}^{2+}$ in blood serum is small compared to blood, and so in water-like liquid layers in the absence of hydrocarbons, the rate of decomposition of $\text{H}_2\text{O}_{2\text{aq}}$ is likely small.

O_3 is another powerful oxidizing agent, which is known for bacterial killing and has been correlated with the biocidal properties of PAW generated by a remote plasma [46]. O_3 has an oxidizing potential of 2.07 eV. When dissolved, $\text{O}_{3\text{aq}}$ can react with and oxidize organic compounds either directly or via radical intermediates such as OH. The densities of O and O_3 in the gas phase are shown in figure 6, from the end of the discharge pulse to the end of the first afterglow period. The densities of $\text{HO}_{2\text{aq}}$ and $\text{O}_{3\text{aq}}$ are also shown at times during the afterglow periods. O is dominantly produced in the gas phase during the current pulse by the dissociation of O_2 by direct electron impact and by excitation transfer from $\text{N}_2(A)$. The O density peaks to $1.5 \times 10^{15} \text{ cm}^{-3}$ at $3 \mu\text{s}$ and quickly decays to $7.3 \times 10^{13} \text{ cm}^{-3}$ at $30 \mu\text{s}$. The majority of O is consumed in the formation of O_3 in the afterglow and is regenerated by the next discharge pulse.

In the absence of hydrocarbons in the gas phase, O_3 is long lived and accumulates on a pulse-to-pulse basis, up to $6 \times 10^{14} \text{ cm}^{-3}$ at 23 ms. This accumulation enables O_3 to diffuse into water and be solvated. Although water is less likely to absorb as much O_3 as H_2O_2 due to the smaller Henry's law constant (0.3) for O_3 , its larger density and continuous flux incident onto the surface of the water results in a large density of $\text{O}_{3\text{aq}}$. As shown in figure 6, the $\text{O}_{3\text{aq}}$ reaches a maximum density of 10^{17} cm^{-3} ($1.6 \times 10^{-4} \text{ M}$), larger than the density of $\text{H}_2\text{O}_{2\text{aq}}$. This large density of $\text{O}_{3\text{aq}}$ is consistent with the rapid rates of ozonation of water by remote plasmas and their subsequent role in bacteria killing [46]. The rate of solvation of O atoms is negligible compared to $\text{O}_{3\text{aq}}$ due to the consumption of O atoms in the gas phase to make O_3 , and there is a negligible production of O_{aq} due to the dissociation of $\text{H}_2\text{O}_{\text{aq}}$. To produce O_{aq} from $\text{H}_2\text{O}_{\text{aq}}$ through either photo-dissociation or electron impact dissociation requires an energy larger than 13.5 eV [47]. As a result, $\text{O}_{3\text{aq}}$ in liquid water results dominantly from the diffusion of O_3 from the gas phase. In the absence of hydrocarbons, $\text{O}_{3\text{aq}}$ is a terminal species and will reach the underlying tissue. Due to its nearly exclusive gas phase source and low reactivity in the water, the solvation and transport of $\text{O}_{3\text{aq}}$ is much the same for both direct and indirect plasma sources.

$\text{HO}_{2\text{aq}}$, shown in figure 6, is dominantly formed at the top of the water layer by H_{aq} combining with dissolved $\text{O}_{2\text{aq}}$.

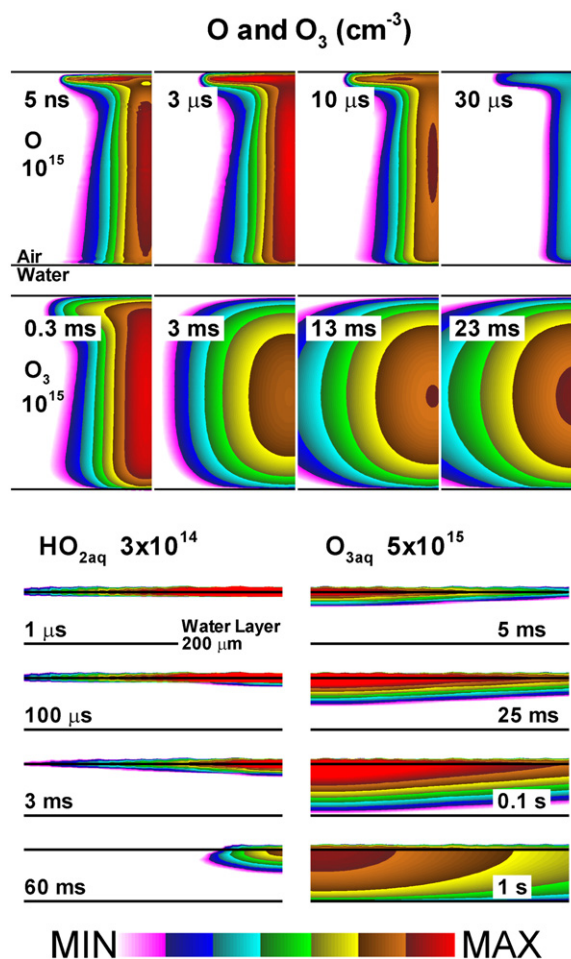


Figure 6. The evolution of ROS densities in the (top) gas gap and (bottom) $200 \mu\text{m}$ water layer. The O density is shown during the first pulse and interpulse afterglow. The O_3 density is shown accumulating after each pulse (0, 10 ms, 20 ms) and during the terminal afterglow. $\text{O}_{3\text{aq}}$ and $\text{HO}_{2\text{aq}}$ are shown in the liquid during the discharge pulses and through the terminal afterglow. The contours are plotted on a three-decade log-scale with the maximum values noted in each frame.

The production of H_{aq} is nearly the same as that of OH_{aq} , as the production of both are dominated by the dissociation of $\text{H}_2\text{O}_{\text{aq}}$, with secondary sources by diffusion of H and OH from the gas phase. The dissociation of $\text{H}_2\text{O}_{\text{aq}}$ is largely due to photo-dissociation at the top of the water layer. Unlike terminal species such as $\text{O}_{3\text{aq}}$, $\text{HO}_{2\text{aq}}$ is a transient species. It is consumed by hydrolysing into $\text{H}_3\text{O}_{\text{aq}}^+$ and $\text{O}_{2\text{aq}}^-$, or assisting NO_{aq} to form $\text{HNO}_{3\text{aq}}$. The maximum density of $\text{HO}_{2\text{aq}}$ is $2 \times 10^{15} \text{ cm}^{-3}$ ($3.3 \times 10^{-6} \text{ M}$). In water layers in contact with air discharges, there can be a large enough density of NO_{aq} that $\text{HO}_{2\text{aq}}$ is more consumed by the formation of $\text{HNO}_{3\text{aq}}$ than by hydrolysis. In remote plasma jets where the fluxes of NO into the water may be low, $\text{HO}_{2\text{aq}}$ will instead hydrolyse and be an important source of $\text{H}_3\text{O}_{\text{aq}}^+$.

The nitrogen oxide chemistry in the water is, for all practical purposes, initiated by gas phase species diffusion into the water as there are few native nitrogen containing species in the water, at least for our conditions. The density of dissolved nitrogen oxide species initially in the water is typically small. There are a variety of nitrogen oxide species (e.g., NO, NO_2 ,

N_2O , N_2O_3 , N_2O_4 , N_2O_5) produced in the gas discharge, which is initiated by the formation of NO. The densities of a selection of these species are shown in figure 7. NO dominates the nitrogen oxide species and is mainly produced in the afterglow. The inventory accumulates during each pulse. Its maximum density increases from $5 \times 10^{13} \text{ cm}^{-3}$ at 3 ms to $8 \times 10^{13} \text{ cm}^{-3}$ at 23 ms. Like O_3 , multiple pulses significantly increase the NO density in the gas phase. N_xO_y , the set of nitrogen species other than NO (e.g., NO_2 , N_2O , N_2O_3 , N_2O_4 , N_2O_5), also follows a similar trend of accumulating pulse to pulse but in general have densities smaller than NO by a factor of 100. The density of N_xO_y increases from $2 \times 10^{11} \text{ cm}^{-3}$ at 3 ms to $5 \times 10^{11} \text{ cm}^{-3}$ at 23 ms. Since N_xO_y originates from the production of NO, the accumulation of NO during each pulse produces a significant increment of N_xO_y .

As the OH density increases with successive pulses due to the dissociation of water, reactions with NO and NO_2 produce HNO_2 , HNO_3 and HOONO, with maximum densities above the water of $8 \times 10^{12} \text{ cm}^{-3}$, $9 \times 10^{11} \text{ cm}^{-3}$ and $4 \times 10^{11} \text{ cm}^{-3}$ at 23 ms. HOONO is produced through reactions of $NO_2 + OH$ and $NO + HO_2$. Both OH and HO_2 originate with H_2O , so the maximum density of HOONO is close to the water surface where the water vapour density is higher. The same formation process applies to HNO_2 and HNO_3 , shown as HNO_x in figure 7. The densities of other nitrogen oxide species are low. All of these species diffuse into the water and hydrolyse. The absorption and solvation processes of acid species (e.g., HNO_2 and HNO_3) from the gas phase into the water are more rapid than for N_xO_y , (e.g., NO and NO_2). As a result, the formation of aqueous acid species can be correlated to gas phase acid formation.

The peroxyxynitrite $ONOO_{aq}^-$ is toxic to cells due to its higher oxidizing potential and its ability to diffuse through several cell diameters and cell walls before reacting [48–50]. It is also able to initiate lipid peroxidation, causing cell wall damage [48–50]. Its conjugate acid, peroxyxynitrous acid or HOONO, can also react with biological molecules through various mechanisms [51]. Although the production of peroxyxynitrous acid in liquid is well known, its production in the gas phase is not clear. Atkinson *et al* [52] suggested that the production of HOONO in the gas phase cannot be ignored, and Nizkorodov and Wennberg [53] made spectroscopic observations of gas-phase HOONO. Both HNO_3 and HOONO are likely produced in the gas phase by reactions of NO_2 with OH, and NO with HO_2 as discussed above [54–56]. When OH reacts with the O atom in ONO (the same as NO_2 but representing the molecular structure), the linear molecule HOONO is produced. When OH reacts with the N atom in ONO, the nonlinear HNO_3 is produced. HOO (the same as HO_2 but representing its molecular structure) also has a linear molecular structure and is more likely to bond with the O atom in NO to form HOONO. In order to form HNO_3 , HO_2 needs to restructure itself.

In experiments [53, 54], HOONO was determined by a ratio of $HOONO/HNO_3$, which ranges from 5% to 30%. Rate coefficients for the reaction of OH and NO_2 , $1.57 \times 10^{-11} \text{ cm}^3 \text{ s}^{-1}$; and for the reaction of HO_2 and NO, $2.31 \times 10^{-13} \text{ cm}^3 \text{ s}^{-1}$ [55, 56], produce a ratio of $HOONO/HNO_3$ of $\approx 40\%$ in the gas phase. The production of HOONO and

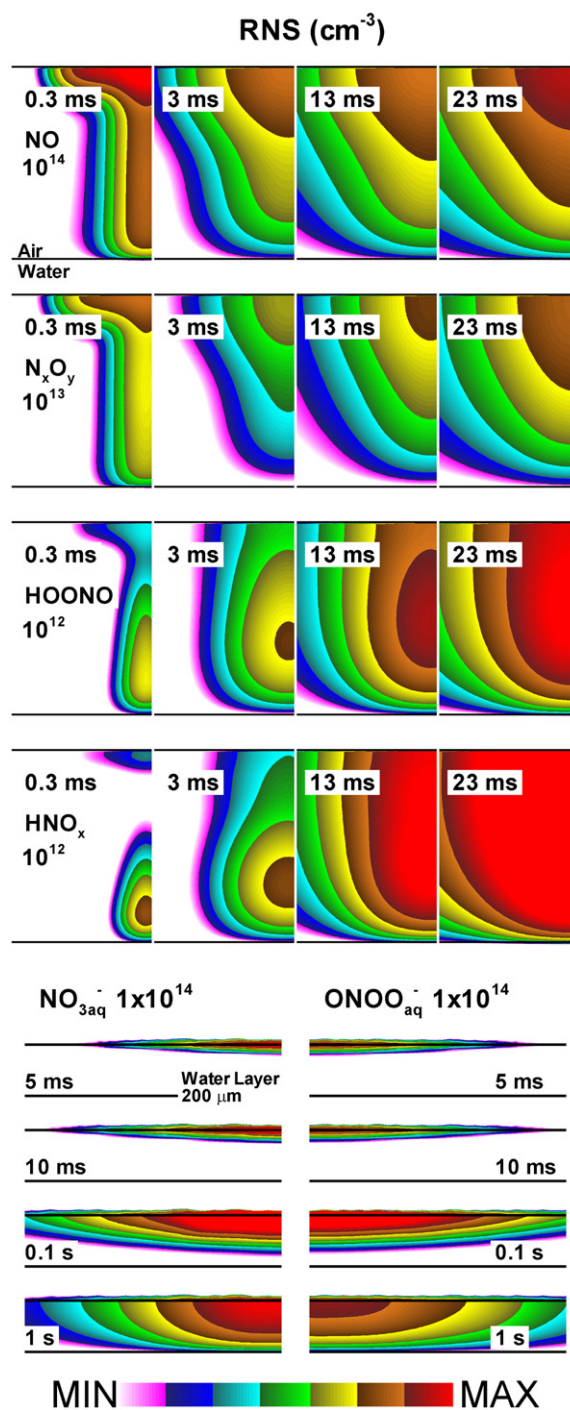


Figure 7. The evolution of RNS densities in the (top) gas gap and (bottom) $200 \mu\text{m}$ water layer. The densities of NO, N_xO_y , HOONO and HNO_x are shown accumulating after each of the three discharge pulses and into the terminal afterglow. In the gas phase, N_xO_y , except for NO, consists of NO_2 , NO_3 , N_2O_3 , N_2O_4 and N_2O_5 ; and HNO_x consists of HNO_2 and HNO_3 . NO dominates the nitrogen oxide species and HNO_2 dominates the nitrogen acid species. In the liquid, $ONOO_{aq}^-$ and NO_{3aq}^- are shown for the terminal afterglow. The contours are plotted on a 3-decade log-scale with the maximum values noted in each frame.

HNO_3 consumes a small portion of the NO and NO_2 . Given the narrow gap between the DBD applicator and the surface of the water, the majority of NO, NO_2 will eventually become solvated in the water and form $HOONO_{aq}$. This solvation

dominates the production of HOONO_{aq} . The solvation of gas phase HOONO accounts for 11% of total HOONO_{aq} production given that HOONO has a much larger Henry's law constant, 4.8×10^6 . In the remote plasma treatment of water, the proportion of reactivity in the water produced by the solvation of gas phase neutral species is larger than for direct plasma treatment where photons and ions make important contributions. As a result, the contribution of gas phase HOONO to the production of HOONO_{aq} is likely more important in remote plasma treatment.

All of these nitrogen oxide species from the gas phase diffuse into the water layer and slowly convert to $\text{HNO}_{x\text{aq}}$ (e.g., $\text{HNO}_{2\text{aq}}$, $\text{HNO}_{3\text{aq}}$ and HOONO_{aq}). $\text{HNO}_{3\text{aq}}$ is primarily formed through reactions of NO_{aq} with $\text{HO}_{2\text{aq}}$ or $\text{NO}_{2\text{aq}}$ with OH_{aq} . Note that both of these channels are sensitive to dissolved $\text{O}_{2\text{aq}}$, and to the photodissociation that produces H_{aq} and OH_{aq} . In an aqueous solution, HOONO_{aq} is formed through the reaction of NO_{aq} and $\text{HO}_{2\text{aq}}$ with rate coefficient $3.2 \times 10^9 \text{M}^{-1} \text{s}^{-1}$ [38] and the reaction of $\text{NO}_{2\text{aq}}$ and OH_{aq} with rate coefficient $1.2 \times 10^{10} \text{M}^{-1} \text{s}^{-1}$ [38]. The former reaction dominates since NO_{aq} is much larger than $\text{NO}_{2\text{aq}}$. We assumed that the branching ratios for the formation of $\text{HNO}_{3\text{aq}}$ is analogous to the gas phase reactions. So the ratio of HOONO_{aq} to $\text{HNO}_{3\text{aq}}$ is also about 40%. $\text{HNO}_{3\text{aq}}$ is also produced in the reaction $\text{NO}_{2\text{aq}} + \text{NO}_{2\text{aq}} + \text{H}_2\text{O}_{\text{aq}}$, however the reaction probability is small and so is not an important process.

$\text{HNO}_{3\text{aq}}$ and HOONO_{aq} quickly hydrolyse in water to form $\text{H}_3\text{O}_{\text{aq}}^+$, $\text{NO}_{3\text{aq}}^-$ and $\text{ONOO}_{\text{aq}}^-$. $\text{ONOO}_{\text{aq}}^-$ has a linear molecular structure and a high oxidizing potential [48]. In addition to the hydrolysis, the reaction between $\text{O}_{2\text{aq}}^-$ and NO_{aq} nearly doubles the production of $\text{NO}_{3\text{aq}}^-$ and $\text{ONOO}_{\text{aq}}^-$. $\text{HNO}_{2\text{aq}}$ is mainly produced by reactions between NO_{aq} and OH_{aq} . Since both NO_{aq} and OH_{aq} have large densities in the liquid, $\text{HNO}_{2\text{aq}}$ dominates over $\text{HNO}_{3\text{aq}}$ and HOONO_{aq} . However, $\text{HNO}_{2\text{aq}}$ is a weaker acid and only about 1% of $\text{HNO}_{2\text{aq}}$ hydrolyses in the water. As a result, the density of the $\text{NO}_{2\text{aq}}^-$ is small, and $\text{HNO}_{2\text{aq}}$ persists longer in water prior to hydrolysing.

As a result of these hydrolysing reactions, $\text{H}_3\text{O}_{\text{aq}}^+$, $\text{NO}_{3\text{aq}}^-$ and $\text{ONOO}_{\text{aq}}^-$ are the major terminal species of RNS diffusion into the water from the gas phase. These species accumulate pulse to pulse in the liquid and eventually diffuse to the tissue. The densities $\text{NO}_{3\text{aq}}^-$ and $\text{ONOO}_{\text{aq}}^-$ during the pulses and at the end of the terminal afterglow are shown in figure 7. At the end of the 1 s afterglow, the density of $\text{NO}_{3\text{aq}}^-$ above the tissue is $4 \times 10^{13} \text{cm}^{-3}$ ($6.7 \times 10^{-8} \text{M}$) and for $\text{ONOO}_{\text{aq}}^-$ is $2 \times 10^{13} \text{cm}^{-3}$ ($3.3 \times 10^{-8} \text{M}$).

The acidification of water by plasma exposure has been observed experimentally. In experiments by Hamaguchi and co-workers [25], the pH value of water decreased from 5.7 to 4.3 in 300 s by plasma jet treatment. Hamaguchi *et al* also found a critical pH of the solution, ≈ 4.7 , below which the bactericidal effect becomes particularly strong. In experiments by Weltman *et al* [57], an indirect surface DBD was used for water treatment, resulting in a decrease of pH from 7 to less than 4 in the first 5 min of plasma treatment, followed by a slight further decrease reaching more or less stable pH values between 2 and 3 within 30 min depending on the sample volume. This acidification of water is important in bacteria

killing. The experimental results by Graves and co-workers [46] showed a strong antibacterial effect in non-buffered PAW and a small antibacterial effect in buffered PAW. Lukes and co-workers [29] also reported that the reactivity of peroxyxynitrites can depend strongly on the pH value and are highly reactive under acidic conditions.

In our model, we assume that all hydronium ions are active ions, so the pH value is determined by the concentration of $\text{H}_3\text{O}_{\text{aq}}^+$. After three pulses, the average pH is 6, whereas after six pulses the average pH is 5.8. Unfortunately, the hydronium ions do not increase in direct proportion to the plasma treatment time. This could be due to neutralizing reactions between electrons and hydronium ions as the density of hydronium ions rises, or could be due to our treating a thin water layer where species react with the underlying tissue. The increment of hydronium ions by successive pulses decreases and the density of hydronium appears to saturate in the long term. We can still make a rough prediction of the long term acidification. Extrapolating our results for 100 pulses, 500 ns of plasma treatment and 1 s total treatment time, the pH value could drop to as low as 4.0. For 30 000 pulses, 150 μs of plasma treatment and 5 min total treatment, the pH value can drop to 3.0, in which the water is significantly acidified. In such an acidic environment, the rate coefficients in our mechanism could be altered.

These just-discussed results are sensitive to a number of factors, both environmental and geometrical. For example, the densities of $\text{H}_2\text{O}_{2\text{aq}}$, $\text{O}_{3\text{aq}}$, $\text{HO}_{2\text{aq}}$ and $\text{ONOO}_{\text{aq}}^-$ are shown in figure 8 for the base case, when excluding photolysis reactions, when excluding dissolved $\text{O}_{2\text{aq}}$ and when including a generic dissolved alkane hydrocarbon RH_{aq} . For plasmas which are in close proximity to (physically in contact with) water, even short mean free path UV/VUV photons are incident onto the water. These photons photolyse the water with nearly unity probability, producing H_{aq} and OH_{aq} . For our conditions, the production of any species that trace their origin to H_{aq} and OH_{aq} is dominated by this photolysis on short times. $\text{H}_2\text{O}_{2\text{aq}}$ comes from the recombination of OH_{aq} , and the formation $\text{HO}_{2\text{aq}}$ depends on H_{aq} . There are few other sources of H_{aq} and OH_{aq} in the water other than diffusion of their gas phase analogues into the water. So $\text{H}_2\text{O}_{2\text{aq}}$ and $\text{HO}_{2\text{aq}}$ are particularly sensitive to photolysis on shorter time scales, and their densities decrease by a factor of 20 in the absence of photolysis. For many seconds to minutes exposure, we expect that the buildup of the gas phase densities of, H, OH and H_2O_2 and their diffusion into the water will bolster the densities of $\text{H}_2\text{O}_{2\text{aq}}$ and $\text{HO}_{2\text{aq}}$ in the absence of photolysis.

$\text{ONOO}_{\text{aq}}^-$ is produced through OH_{aq} reacting with $\text{NO}_{2\text{aq}}$, and $\text{HO}_{2\text{aq}}$ reacting with NO_{aq} , and so $\text{ONOO}_{\text{aq}}^-$ is also sensitive to photolysis. However, there are other sources of $\text{ONOO}_{\text{aq}}^-$. As mentioned above, HOONO is produced in the gas phase and is then solvated in water and eventually hydrolysed to $\text{ONOO}_{\text{aq}}^-$. The production of the precursors to HOONO in the gas phase is very sensitive to the gas humidity (not shown here), and so small changes in humidity will correlate with changes in $\text{ONOO}_{\text{aq}}^-$. The solvation of HOONO in the afterglow contributes 11% to the production of HOONO_{aq} . $\text{O}_{3\text{aq}}$ is less sensitive to the absence of UV/VUV fluxes as O atoms are

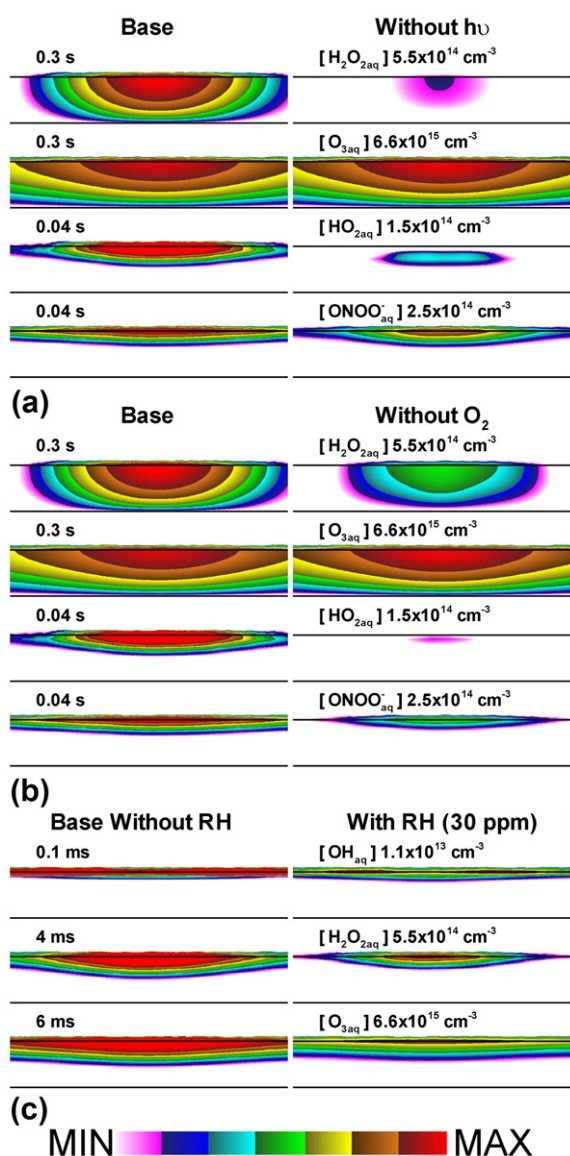


Figure 8. Comparison of radical densities in the 200 μm water layer under different conditions. The base case is for three discharge pulses at 100 Hz over water with 8 ppm $\text{O}_{2\text{aq}}$ and with UV/VUV illumination. The densities of $\text{H}_2\text{O}_{2\text{aq}}$, $\text{O}_{3\text{aq}}$, $\text{HO}_{2\text{aq}}$ and $\text{ONOO}_{\text{aq}}^-$ are shown for (a) the base case compared to without photon reactions in the water, and (b) the base case compared to degassed water without dissolved $\text{O}_{2\text{aq}}$. (c) The densities of $\text{H}_2\text{O}_{2\text{aq}}$, $\text{O}_{3\text{aq}}$ and OH_{aq} for the base case without dissolved hydrocarbon RH compared to a water layer with RH of 30 ppm. The contours are plotted on a three-decade log-scale with the maximum values noted in each frame.

not directly produced in large numbers by photolysis. $\text{O}_{3\text{aq}}$ is generated dominantly by the diffusion of O_3 from the gas phase.

When excluding $\text{O}_{2\text{aq}}$, the production of $\text{HO}_{2\text{aq}}$ is severely diminished as its major source is the reaction of photolysis produced H_{aq} with $\text{O}_{2\text{aq}}$. One unintended consequence is that large densities of H_{aq} persist in the absence of $\text{O}_{2\text{aq}}$. Although not overly important, these H_{aq} reduce the density of OH_{aq} by recombination. The density of $\text{ONOO}_{\text{aq}}^-$ is also reduced in the absence of $\text{O}_{2\text{aq}}$ due to the lack of reactions between OH_{aq} and $\text{HO}_{2\text{aq}}$. The production of $\text{H}_2\text{O}_{2\text{aq}}$ is not directly associated

with $\text{O}_{2\text{aq}}$, however the large amount of otherwise slowly reacting H_{aq} recombines with OH_{aq} to reduce the feedstock reactants which form $\text{H}_2\text{O}_{2\text{aq}}$. Again, $\text{O}_{3\text{aq}}$ is not affected by a lack of dissolved $\text{O}_{2\text{aq}}$ since little $\text{O}_{3\text{aq}}$ is produced by reactions between O_{aq} and $\text{O}_{2\text{aq}}$ —little O from the gas phase avoids forming O_3 to diffuse into the water.

The presence of dissolved hydrocarbons in the liquid, in our case a generic alkane RH_{aq} , can have a major impact on ROS. These hydrocarbons are basic organic compounds containing only carbon and hydrogen. ROS most commonly reacts with RH_{aq} by H-atom abstraction from the C–H bond to form an alkyl radical, $\text{R}_{\text{aq}}\cdot$. The reaction of ROS with RH_{aq} occurs at rates approaching EGK. For example, the reaction of OH_{aq} with simple hydrocarbons proceeds at rates of 10^7 – $10^9 \text{M}^{-1} \text{s}^{-1}$ (10^{-14} – $10^{-12} \text{cm}^3 \text{s}^{-1}$) [41, 42]. The rate coefficients of the reactions of $\text{H}_2\text{O}_{2\text{aq}}$ and $\text{O}_{3\text{aq}}$ with RH_{aq} , though smaller than for OH_{aq} , are significant: 10^5 – $10^8 \text{M}^{-1} \text{s}^{-1}$ (10^{-16} – $10^{-13} \text{cm}^3 \text{s}^{-1}$). To provide perspective, if an ROS species has a rate coefficient of $10^7 \text{M}^{-1} \text{s}^{-1}$ for reaction with an RH_{aq} having a density of 1 ppm (parts-per-million) in water, the reaction time is about 2 ms. So it is expected that ROS will be sensitive to even small amounts of RH_{aq} .

The densities of $\text{H}_2\text{O}_{2\text{aq}}$, $\text{O}_{3\text{aq}}$ and $\text{HO}_{2\text{aq}}$ are shown in figure 8 for 30 ppm of RH_{aq} . For all practical purposes, these species do not penetrate beyond the surface layers of the water. The reactivity that the ROS bring to the water is converted to $\text{R}_{\text{aq}}\cdot$. Of course, the precise identify of $\text{R}_{\text{aq}}\cdot$ depends on the type of RH_{aq} . There will also likely be subsequent reactions of $\text{R}_{\text{aq}}\cdot$ with other RH_{aq} and solvated species. For long chain alkanes, it is also possible that there will be multiple hydrogen abstractions from the alkane to produce multiple free radical sites. The important point is that for biological liquids where there is a significant mole fraction of hydrocarbons, the vast majority of ROS likely reacts with the dissolved hydrocarbons before reaching the underlying tissue, with the majority of that reactivity being initially converted to $\text{R}_{\text{aq}}\cdot$. In another scenario, RH_{aq} may protect against cell damage by ROS. Once generated, $\text{R}_{\text{aq}}\cdot$ has many potential outcomes. $\text{R}_{\text{aq}}\cdot$ may abstract hydrogen from a protective agent and be restored to its original state [58] or may acquire an electron from other molecules, which prominently involves diffusible thiol compounds, such as glutathione [59]. $\text{R}_{\text{aq}}\cdot$ may also combine with $\text{O}_{2\text{aq}}$, resulting in the formation of a peroxy radical, $\text{ROO}_{\text{aq}}\cdot$. The $\text{ROO}_{\text{aq}}\cdot$ is able to react with another hydrocarbon RH_{aq} molecule to form ROOH_{aq} and propagate the chain to produce another $\text{R}_{\text{aq}}\cdot$ [60]. For our conditions, this reaction chain proceeds slowly on time scales beyond what was considered here. In order for ROS activity from the gas phase to directly reach the tissue, a long term plasma treatment is necessary to produce more ROS to completely consume the RH_{aq} . In our model with thin water layers, at least 30 000 pulses—a 5 min treatment—would be needed to consume the RH_{aq} .

The time-dependent densities of solvated neutral species at the surface of the water directly under the impact point of the streamer are shown in figure 9. The time axis was rescaled to be relative to the start of each discharge pulse. Charged particle densities are shown in figure 9(a). The initial fluxes of

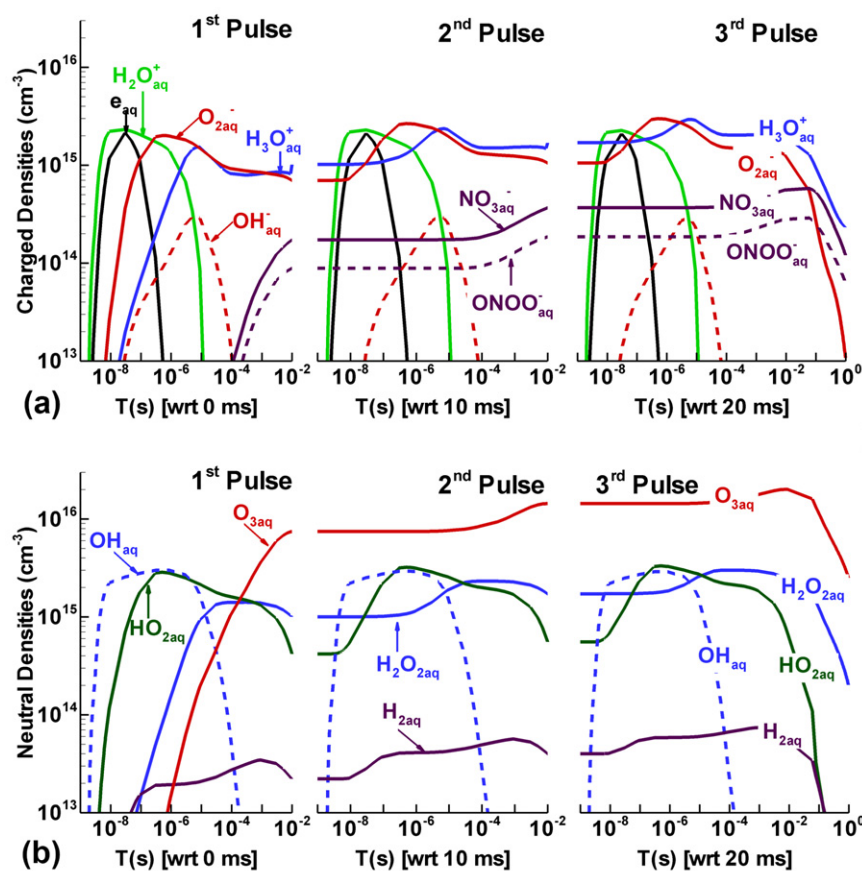


Figure 9. The time evolution of (a) charged and (b) neutral densities at the top surface of the 200 μm water layer over three discharge pulses. The time axis in each plot is relative to the start of the first, second and third discharge pulse.

charged species into the water are electrons and water ions. All electrons striking the liquid are rapidly solvated to form e_{aq} , whose density rises in 5 ns corresponding with the avalanche time of the discharge. The density of e_{aq} rapidly drops due in large part to the attachment to dissolved $\text{O}_{2\text{aq}}$, which produces the increase in the density of $\text{O}_{2\text{aq}}^-$. The water ions, $\text{H}_2\text{O}_{\text{aq}}^+$, decay slower than electrons. They react with $\text{H}_2\text{O}_{\text{aq}}$ to form $\text{H}_3\text{O}_{\text{aq}}^+$, and meanwhile OH_{aq} is produced. The density of $\text{H}_3\text{O}_{\text{aq}}^+$ rises later than that of $\text{O}_{2\text{aq}}^-$ but eventually reaches the same level as $\text{O}_{2\text{aq}}^-$, and so the macroscopic neutrality of water layer is maintained. The densities of $\text{NO}_{3\text{aq}}^-$ and $\text{OONO}_{\text{aq}}^-$ increase late in the afterglow of the first pulse due to the slower formation of nitrogen oxide species in the gas phase during the afterglow. Following the second and third pulses, the long lived species $\text{O}_{2\text{aq}}^-$, $\text{H}_3\text{O}_{\text{aq}}^+$, $\text{NO}_{3\text{aq}}^-$ and $\text{OONO}_{\text{aq}}^-$ accumulate. During the terminal afterglow following the third pulse, the densities of all species decrease due to diffusion through the water to the underlying tissue.

The densities of neutral species are shown in figure 9(b). The density of OH_{aq} has a sharp rise in 5 ns due to the photolysis of liquid water and a slow increase over many μs due to the diffusion and solvation of OH from the gas phase. The reaction of $\text{H}_2\text{O}_{\text{aq}}^+$ and $\text{H}_2\text{O}_{\text{aq}}$ also contributes about 27% to the initial rise of OH_{aq} . The mutual reaction of OH_{aq} to form $\text{H}_2\text{O}_{2\text{aq}}$ results in the decrease of OH_{aq} and the rise of $\text{H}_2\text{O}_{2\text{aq}}$. The density of $\text{O}_{3\text{aq}}$ continues to rise during each

pulse as the fluence of O_3 from the gas phase increases. In the absence of organic matter, $\text{O}_{3\text{aq}}$ is relatively stable and so its density accumulates until depleted by diffusion. $\text{HO}_{2\text{aq}}$, is a transient agent which assists in the production of nitric and peroxyxynitrous acids. Although $\text{HO}_{2\text{aq}}$ reaches a high density, it is consumed eventually through these acid forming reactions. $\text{H}_{2\text{aq}}$ follows the same trend of $\text{H}_2\text{O}_{2\text{aq}}$. Because H_{aq} is consumed in the formation of $\text{HO}_{2\text{aq}}$, the $\text{H}_{2\text{aq}}$ density is quite low. During the terminal afterglow, the densities of these neutral species fall due to diffusion into the water layer.

Reuter and co-workers [61] reported on quantitative measurements of OH_{aq} and $\text{O}_{2\text{aq}}^-$ in aqueous solution after plasma treatment. In their experiment, the OH_{aq} density is as large as $1.8\mu\text{M}$ after a 3 min plasma treatment, then it decreases to $0.25\mu\text{M}$ in 20 h and remains constant for 74 h. Our results show that the OH_{aq} density at the top of the water peaks at $3.2\mu\text{M}$ and then falls to $0.01\mu\text{M}$ after 0.1 ms. The conversion of OH_{aq} to $\text{H}_2\text{O}_{2\text{aq}}$ in our model using conventional rate coefficients is much faster than reported in their experiment. This may be due to the DMPO/OH adduct in the experiment, which traps the OH_{aq} and slows down the conversion to $\text{H}_2\text{O}_{2\text{aq}}$. The peak value of OH_{aq} density in our model is close to that in the experiment; however, taking into account the short plasma treatment in our model, the OH_{aq} production rate is larger than that in the experiment. This is also consistent given that we

Table 3. Contributions of reactions to aqueous radical production.

Species	Reactions	Contribution
OH _{aq}	$h\nu + \text{H}_2\text{O}_{\text{aq}} \rightarrow \text{H}\cdot_{\text{aq}} + \cdot\text{OH}_{\text{aq}}$	39%
	$\text{H}_2\text{O}_{\text{aq}}^+ + \text{H}_2\text{O}_{\text{aq}} \rightarrow \text{H}_3\text{O}_{\text{aq}}^+ + \cdot\text{OH}_{\text{aq}}$	28%
	$\text{H}_3\text{O}_{\text{aq}}^+ + \text{OH}_{\text{aq}}^- \rightarrow \cdot\text{H}_{\text{aq}} + \cdot\text{OH}_{\text{aq}} + \text{H}_2\text{O}_{\text{aq}}$	25%
	$e_{\text{aq}} + \text{H}_2\text{O}_{\text{aq}}^+ \rightarrow \text{H}\cdot_{\text{aq}} + \text{OH}_{\text{aq}}$	4%
	$\text{OH} + \text{H}_2\text{O}_{\text{aq}} \rightarrow \text{OH}_{\text{aq}} + \text{H}_2\text{O}_{\text{aq}}$	3%
	$\text{H}_2\text{O}_{\text{aq}} + \text{H}_2\text{O}_{2\text{aq}} \rightarrow \text{H}\cdot_{\text{aq}} + \cdot\text{OH}_{\text{aq}} + \text{H}_2\text{O}_{\text{aq}}$	1%
H ₂ O _{2aq}	$\cdot\text{OH}_{\text{aq}} + \cdot\text{OH}_{\text{aq}} \rightarrow \text{H}_2\text{O}_{2\text{aq}}$	88%
	$\text{H} + \text{HO}_{2\text{aq}} \rightarrow \text{H}_2\text{O}_{2\text{aq}}$	8%
	$\text{H}_2\text{O}_2 + \text{H}_2\text{O}_{\text{aq}} \rightarrow \text{H}_2\text{O}_{2\text{aq}} + \text{H}_2\text{O}_{\text{aq}}$	4%
HO _{2aq}	$\text{H}\cdot_{\text{aq}} + \text{O}_{2\text{aq}} \rightarrow \text{HO}_2\cdot_{\text{aq}}$	100%
O _{3aq}	$\text{O}_3 + \text{H}_2\text{O}_{\text{aq}} \rightarrow \text{O}_{3\text{aq}} + \text{H}_2\text{O}_{\text{aq}}$	100%
HNO _{2aq}	$\text{HNO}_2 + \text{H}_2\text{O}_{\text{aq}} \rightarrow \text{HNO}_{2\text{aq}} + \text{H}_2\text{O}_{\text{aq}}$	40%
	$\text{NO}_{\text{aq}} + \cdot\text{OH}_{\text{aq}} \rightarrow \text{HNO}_{2\text{aq}}$	27%
	$\text{N}_2\text{O}_{3\text{aq}} + \text{H}_2\text{O}_{\text{aq}} \rightarrow \text{HNO}_{2\text{aq}} + \text{HNO}_{2\text{aq}}$	26%
	$\text{NO}_{\text{aq}} + \text{NO}_{2\text{aq}} + \text{H}_2\text{O}_{\text{aq}} \rightarrow \text{HNO}_{2\text{aq}} + \text{HNO}_{2\text{aq}}$	7%
HNO _{3aq}	$\text{NO}_{\text{aq}} + \text{HO}_2\cdot_{\text{aq}} \rightarrow \text{HNO}_{3\text{aq}}$	89%
	$\text{HNO}_3 + \text{H}_2\text{O}_{\text{aq}} \rightarrow \text{HNO}_{3\text{aq}} + \text{H}_2\text{O}_{\text{aq}}$	11%
HOONO _{aq}	$\text{NO}_{\text{aq}} + \text{HO}_2\cdot_{\text{aq}} \rightarrow \text{HOONO}_{\text{aq}}$	89%
	$\text{HOONO} + \text{H}_2\text{O}_{\text{aq}} \rightarrow \text{HOONO}_{\text{aq}} + \text{H}_2\text{O}_{\text{aq}}$	11%

are modelling the direct plasma exposure of the water and the experiment is for remote exposure. Reuter and co-workers [61] also measured the O_{2aq}⁻ and concluded that O_{2aq}⁻ is more stable than OH_{aq}, which is consistent with our predicted results.

The aqueous radical production channels and their relative contributions are shown in table 3. These results were produced by integrating the rate of production over the entire water volume for 1 s and then normalizing to the total production rate. Photodissociation is the major source of OH_{aq}, accounting for 39% of total production, although photodissociation lasts for only tens of ns. Charge exchange (H₂O_{aq}⁺ reacting with H₂O_{aq}) and ion recombination (H₃O_{aq}⁺ reacting with OH_{aq}⁻) have contributions of 28% and 25%, respectively. Since H₂O_{aq}⁺ is largely produced by photoionization, the charge exchange source of OH_{aq} traces its origin to photoionization. Therefore, the photon-induced production of OH_{aq} contributes almost 70% of the total. Electron recombination (e_{aq} and H₂O_{aq}⁺) lasts for only several ns, and contributes 4% to the production of OH_{aq}. The solvation of OH through diffusion from the gas phase contributes 3%, but lasts for milliseconds and is the dominant source during the interpulse period. Since the majority of OH in a narrow gap system will eventually be solvated in the liquid layer, the contribution to solvation depends largely on the OH density produced in the gas phase. In global modelling of repetitively pulsed DBDs in humid air for similar conditions, the density of OH reaches a quasi-steady state value of 10¹² for low power deposition [24] and 10¹³ cm⁻³ for high power deposition after tens of pulses [62], which is commensurate with the few pulse values calculated here. So for direct plasma exposure with narrow gaps, the proportion of OH_{aq} produced by direct solvation by OH is likely small. For remote plasma exposure, the solvation of OH is likely to be the dominant source of OH_{aq}.

H₂O_{2aq} is dominantly produced through the mutual reaction of OH_{aq}, 88% of the total, which is also the major sink of OH_{aq}. OH_{aq} is also consumed though reacting with

NO_{aq} and NO_{2aq}. Since NO and NO₂ require milliseconds to diffuse to and solvate in the water, the majority of OH_{aq} has already converted to H₂O_{2aq}. Under quasi-steady state operation, the proportion of OH_{aq} consumed by reactions with NO_{aq} and NO_{2aq} is likely higher. The reaction of H_{aq} with HO_{2aq} and the solvation of H₂O₂ contribute the remaining 8% and 4%, respectively. HO_{2aq} is dominantly produced through H_{aq} reacting O_{2aq} in the liquid layer—essentially 100%. Different to HO_{2aq}, O_{3aq} is produced only through gas phase solvation processes.

Aqueous RNS basically comes from the reaction of OH_{aq} and HO_{2aq} with NO_{aq} and NO_{2aq}. The solvation of HNO₂ is the major source for producing HNO_{2aq}: 40% of total production. In the gas phase, the three-body reaction, NO+OH+M, produces 10¹² cm⁻³ of HNO₂, one order of magnitude higher than HNO₃ and HOONO. So the solvation process is significant. OH_{aq} reacting with NO_{aq}, and N₂O_{3aq} reacting with H₂O_{aq}, produce 27% and 26% of HNO_{2aq}, respectively. The three-body reaction, NO_{aq} + NO_{2aq} + H₂O_{aq}, contributes only 10%. HNO_{3aq} and HOONO_{aq} have similar production channels in which NO_{aq} reacting with HO_{2aq} dominates due to the higher density of NO_{aq} compared to NO_{2aq}. The contribution of this reaction to the production of HNO_{3aq} and HOONO_{aq} is 89%. The solvation of HNO₃ and HOONO both contribute 11% to the total production. A third reaction, NO_{2aq}+NO_{2aq}+H₂O_{aq}, also contributes to HNO_{3aq} production. However, this reaction is quite slow. Nevertheless, it may become more significant in the long term when more NO₂ is produced in the gas phase and especially after the HO_{2aq} is exhausted. Similar to OH_{aq} production, HNO_{3aq} and HOONO_{aq} are more likely to be produced in the liquid phase rather than by solvation.

Since HNO_{3aq} and HOONO_{aq} are strong acids, they almost completely hydrolyse to ions, NO_{3aq}⁻ and ONOO_{aq}⁻, respectively. The production channels of these ions are therefore also represented by the production channels of their conjugate acids. NO_{3aq}⁻ can also result from the reaction of

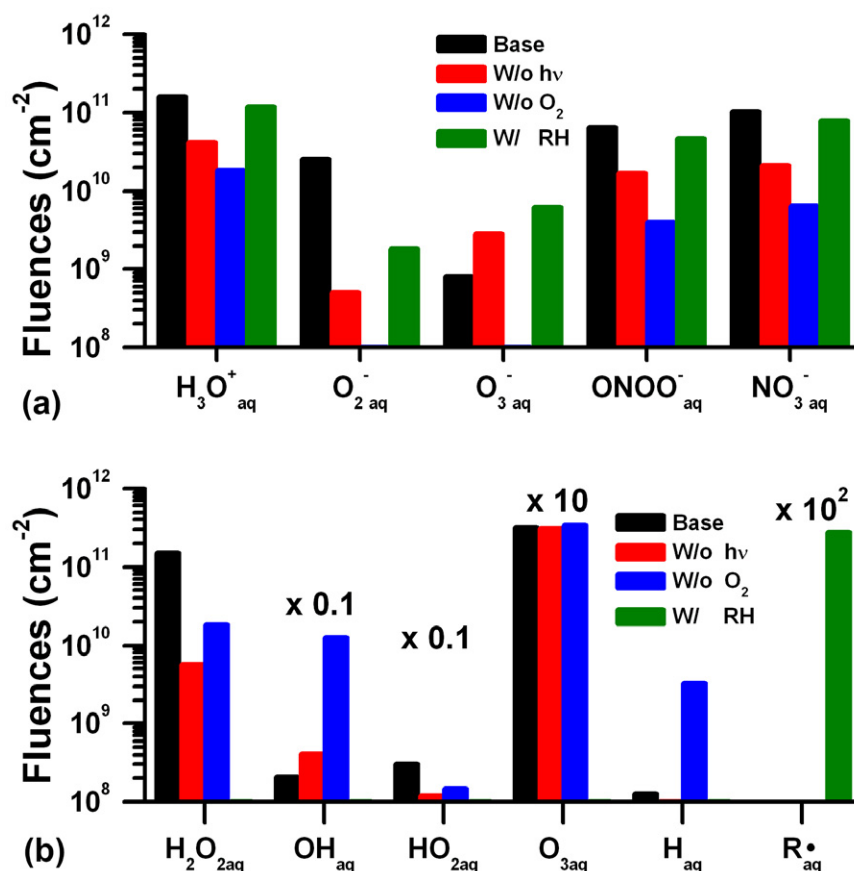


Figure 10. Integrated fluences of (a) charged and (b) neutral species over 1 s onto the tissue underlying the $200 \mu\text{m}$ water layer. Results are shown for the base case, without UV/VUV fluxes, without dissolved $\text{O}_{2\text{aq}}$ and with 30 ppm RH. The ROS fluences are very sensitive to the presence of organic matter in the water.

NO_{aq} and $\text{O}_{2\text{aq}}^-$, which almost doubles its production, resulting in $\text{NO}_{3\text{aq}}^-$ being the major negative ion in the liquid.

In treating liquid covered tissue, it is the fluences (time integrated fluxes) of the species that transport through the liquid layer to the tissue that determine the outcome. As we have discussed, even thin layers of water over tissue can significantly reformat the character of the reactivity produced in the gas phase prior to that reactivity reaching the underlying tissue. To examine these fluences, the fluxes of selected species incident onto the underlying tissue were integrated over the discharge three pulses and the 1 s treatment time of the simulation. We represented the tissue as a lossy dielectric with which all aqueous radicals had a unity reaction probability. We did not include reaction products back into the liquid. The fluences of selected charged and neutral species incident onto the surface for the base case, without photolysis, without dissolved $\text{O}_{2\text{aq}}$ and when having 30 ppm of RH_{aq} , are shown in figure 10. The majority of RNS incident onto the tissue are in the form of negative ions, dominantly $\text{ONOO}_{\text{aq}}^-$ and $\text{NO}_{3\text{aq}}^-$, whose fluences exceed 10^{11}cm^{-2} . There are 10^{15} sites cm^{-2} on, for example, a lipid layer that might cover a cell. So nearly every site on the cell would receive an RNS negative ion after a few thousand pulses. The treatment of such surfaces is therefore likely not to be flux limited but is rather reaction rate limited. The RNS species are not extremely sensitive to the presence of RH_{aq} . Since aqueous RNS results from the

diffusion of the gas phase RNS into the liquid and RNS is not particularly reactive with RH_{aq} , once hydrolysed the RNS simply diffuses through the water layer. Although $\text{HO}_{2\text{aq}}$ can react with RH_{aq} , the reaction is very slow. $\text{HO}_{2\text{aq}}$ reacts with NO_{aq} to form RNS more rapidly than when reacting with RH_{aq} . The RNS is sensitive to a lack of UV/VUV photons and the presence of $\text{O}_{2\text{aq}}$. Since $\text{HO}_{2\text{aq}}$ is a precursor to HOONO_{aq} , which then quickly hydrolyses, the fluences of RNS negative ions is reduced in the absence of UV/VUV photons or $\text{O}_{2\text{aq}}$. $\text{H}_3\text{O}_{\text{aq}}^+$ is similarly insensitive to these variations since its production is supported by the hydrolysis of HNO_{aq} .

With the exception of $\text{O}_{3\text{aq}}$, the fluences of ROS are sensitive to all variables. The fluences of ROS after three discharge pulses and 1 s afterglow are generally 10^{10} – 10^{11}cm^{-2} , similar to RNS. Photolysis, which produces OH_{aq} , is an initiator of reactions which result in $\text{H}_2\text{O}_{2\text{aq}}$ and $\text{HO}_{2\text{aq}}$, and so the absence of photolysis decreases the fluences of these species by more than a factor of 10. The absence of $\text{O}_{2\text{aq}}$ most directly affects the fluences of $\text{HO}_{2\text{aq}}$, reducing its fluence by a factor of 200. The fluence of H_{aq} has the opposite trend, increasing in the absence of $\text{O}_{2\text{aq}}$ due to a lack of the reaction that produces $\text{HO}_{2\text{aq}}$. H_{aq} further recombines with $\text{H}_2\text{O}_{2\text{aq}}$ and reduces $\text{H}_2\text{O}_{2\text{aq}}$ fluences. Meanwhile, the fluence of OH_{aq} is compensated since the recombination produces OH_{aq} . However, the sum of the fluence OH_{aq} and $\text{H}_2\text{O}_{2\text{aq}}$ is reduced. The fluence of $\text{O}_{3\text{aq}}$, 10^{13}cm^{-2} , is the largest of any

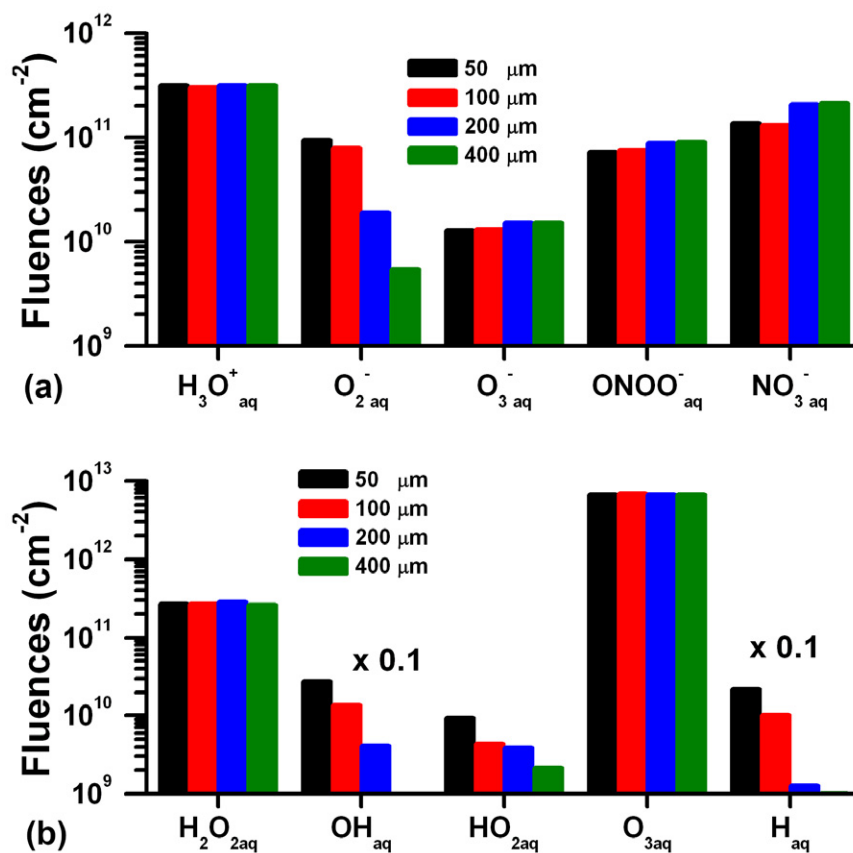


Figure 11. Integrated fluences of (a) charged and (b) neutral species over times up to 20 s onto the tissue underlying the water layers from 50 μm to 400 μm thick. In each case, the three discharge pulses produce nearly the same gas phase fluxes onto the top of the water layer. Species that slowly react (such as $\text{O}_{2\text{aq}}^-$) are consumed in the thicker layer and so their fluences decrease with increasing thickness. Rapidly reacting species, such as OH_{aq} , reach the tissue for thin layers but not for thick layers.

ROS or RNS by a factor of nearly 100 and is nearly insensitive to the absence of photolysis or $\text{O}_{2\text{aq}}$, since $\text{O}_{3\text{aq}}$ originates from the diffusion of O_3 into the liquid. So even if the reactivity of $\text{O}_{3\text{aq}}$ with the underlying tissue is a small fraction of other ROS or RNS, its large fluence may enable significant influence.

The largest uncertainty in this analysis is the influence of RH_{aq} . When including 30 ppm of RH_{aq} , essentially all ROS reactivity is converted to $\text{R}\cdot_{\text{aq}}$, whose fluence to the tissue exceeds 10^{13} cm^{-2} . Biological fluids have orders of magnitude more organic material in the liquid than used in this analysis. The reaction sequences with RH_{aq} forming $\text{R}\cdot_{\text{aq}}$ initiated by solvated ROS are likely to be as important as the form of the ROS that is incident onto the liquid from the gas phase. In our previous discussion, we predict that a 5 min plasma treatment is necessary for the ROS to *burn through* the RH_{aq} . Here we assume that in the reaction with the ROS only one H atom is abstracted from RH_{aq} , but actually RH_{aq} could have multiple H atoms abstracted, resulting in more consumption of the ROS. In this scenario, it would be difficult for the plasma produced ROS to reach the underlying tissue. Again, it would be $\text{R}\cdot_{\text{aq}}$ that reaches the underlying tissue in the interim.

Fluences to the underlying tissue are shown in figure 11 for thicknesses of the liquid layer of 50–400 μm and otherwise for the base case conditions. The post-discharge integration times were chosen to be sufficiently long that the majority of radicals reached the underlying tissue regardless of thickness.

In DBDs, the liquid layer serves as a dielectric which is in series with the applicator dielectric. From 50 to 400 μm , the capacitance of the water layer decreases, but overall the change in radical production is not large. The changes in fluence to the tissue are dominantly attributed to reactions in the liquid layer.

The fluence of OH_{aq} decreases from $2.7 \times 10^9 \text{ cm}^{-2}$ for the 50 μm layer to $1 \times 10^8 \text{ cm}^{-2}$ for the 400 μm layer. OH_{aq} is produced mainly at the top surface of the liquid layer and quickly converts to $\text{H}_2\text{O}_{2\text{aq}}$. For the 50 μm liquid layer, a significant amount of OH_{aq} can reach the underlying tissue before the conversion to $\text{H}_2\text{O}_{2\text{aq}}$, while OH_{aq} is nearly completely converted for the thicker 400 μm layer. In the thicker layer, OH_{aq} is also more likely to be consumed by NO_{aq} . The fluence of $\text{H}_2\text{O}_{2\text{aq}}$ decreases slightly from $2.8 \times 10^{11} \text{ cm}^{-2}$ in the 200 μm liquid layer to $2.6 \times 10^{11} \text{ cm}^{-2}$ in the 50 μm liquid layer due to the loss of OH_{aq} . The fluence of $\text{H}_2\text{O}_{2\text{aq}}$ in the 400 μm layer, $2.5 \times 10^{11} \text{ cm}^{-2}$, is also slightly smaller than that in the 200 μm layer due to $\text{H}_2\text{O}_{2\text{aq}}$ reacting with H_{aq} . However, these differences are small. The reaction of H_{aq} and $\text{H}_2\text{O}_{2\text{aq}}$ produces OH_{aq} , which compensates for other OH_{aq} losses. The fluences of $\text{HO}_{2\text{aq}}$ decrease from $9.2 \times 10^9 \text{ cm}^{-2}$ to $2.2 \times 10^9 \text{ cm}^{-2}$ with an increase of layer thickness. $\text{HO}_{2\text{aq}}$ tends to slowly hydrolyse and react with NO_{aq} , so a thicker water layer provides more opportunity for $\text{HO}_{2\text{aq}}$ to react through these channels before reaching the tissue. The fluence of H_{aq}

decreases from $2.2 \times 10^9 \text{ cm}^{-2}$ to $4 \times 10^7 \text{ cm}^{-2}$ with increasing layer thickness due to its conversion to $\text{H}_{2\text{aq}}$ and reaction with $\text{H}_2\text{O}_{2\text{aq}}$. Since $\text{O}_{3\text{aq}}$ is only produced through solvation and, in the absence of RH_{aq} , has few reactions in the water, its fluence is basically the same for all thicknesses: $6.7 \times 10^{12} \text{ cm}^{-2}$. The small differences are attributed to differences in O_3 production in the gas phase.

The fluences of $\text{H}_3\text{O}_{\text{aq}}^+$, $\text{O}_{3\text{aq}}^-$ and $\text{ONOO}_{\text{aq}}^-$ are nearly the same for different thicknesses of the water layer: about $3 \times 10^{11} \text{ cm}^{-2}$, $1.5 \times 10^{10} \text{ cm}^{-2}$, $8 \times 10^{10} \text{ cm}^{-2}$, respectively. In the absence of RH_{aq} , these ions are quite stable in the liquid. The small differences in $\text{ONOO}_{\text{aq}}^-$, decreasing with decreasing thickness, are attributed to OH_{aq} , which is a precursor producing $\text{ONOO}_{\text{aq}}^-$. In the thinner liquid layer, OH_{aq} is consumed by the underlying tissue so the fluences of $\text{ONOO}_{\text{aq}}^-$ decrease. $\text{O}_{3\text{aq}}^-$ is produced by the reaction of $\text{O}_{2\text{aq}}$ and O_{aq}^- , in which O_{aq}^- traces its origin to OH_{aq} . So the small differences in $\text{O}_{3\text{aq}}^-$ are also attributed to the consumption of OH_{aq} . An increase in the thickness of the water layer extends the residence time of radicals before reaching the underlying tissue. The fluence of $\text{O}_{2\text{aq}}^-$ decreases and the fluence of $\text{NO}_{3\text{aq}}^-$ increases with increasing thickness. During the longer residence time, NO_{aq} is continually refreshed by solvation from the gas phase while $\text{O}_{2\text{aq}}^-$ reacts with NO_{aq} to produce $\text{NO}_{3\text{aq}}^-$. With thin liquid layers, the majority of $\text{O}_{2\text{aq}}^-$ reaches the tissue before sufficient NO_{aq} is solvated to react with it.

4. Concluding remarks

DBDs in contact with water and radical production mechanisms in the adjacent water layers overlying tissue were discussed using results from a computational investigation. The discharges were operated at -18 kV with three pulses followed by a 1–20 s afterglow. Water evaporation from the liquid layer was taken into account and significantly enhances the OH and H_2O_2 production in the gas phase. Plasma produced species, especially neutral ROS and RNS, diffuse onto the water surface and are quickly solvated as determined by Henry's law constants. In some cases, solvated species are determined dominantly by gas phase processes. For example, O_3 is dominantly produced in the gas phase and diffuses into the liquid to become aqueous ozone. Through either charge exchange or attachment processes, charged species, including electrons, eventually become $\text{O}_{2\text{aq}}^-$, $\text{NO}_{3\text{aq}}^-$ and $\text{H}_3\text{O}_{\text{aq}}^+$, which are terminal species and dominate the aqueous ions in the water. UV/VUV radiation from the DBD filaments produces photoionization and photodissociation of the water at the liquid surface, and plays a significant role in producing OH radicals and hydrogen atoms, which are responsible for initiating many reactions in the water. Species such as $\text{H}_2\text{O}_{2\text{aq}}$ and $\text{HO}_{2\text{aq}}$, which trace their origin to OH_{aq} and H_{aq} , are strongly affected by photolysis. By blocking UV/VUV photons, the densities of these species are reduced by more than 50%. These observations are consistent with measurements by Tresp and Reuter, who have shown that VUV illumination of a buffered solution during plasma jet exposure can produce significant quantities of OH and O_2^- through photolysis, and in some

cases dominate production [63]. Dissolved $\text{O}_{2\text{aq}}$ aids in the production of ROS as well as $\text{NO}_{3\text{aq}}^-$ and $\text{ONOO}_{\text{aq}}^-$. The formation of $\text{HO}_{2\text{aq}}$ relies on $\text{O}_{2\text{aq}}$ combining with H_{aq} . $\text{O}_{2\text{aq}}^-$, formed by attachment by $\text{O}_{2\text{aq}}$ from solvated electrons, is a precursor to $\text{NO}_{3\text{aq}}^-$ and $\text{ONOO}_{\text{aq}}^-$.

In the absence of dissolved hydrocarbons, the dominant ROS species reaching the underlying tissue after a few seconds are $\text{H}_2\text{O}_{2\text{aq}}$ and $\text{O}_{3\text{aq}}$. RNS fluences are dominated by $\text{NO}_{3\text{aq}}^-$ and $\text{ONOO}_{\text{aq}}^-$. The ROS fluences are sensitive to dissolved hydrocarbons. A significant RH_{aq} density will consume most ROS, converting their reactivity to a fluence of R_{aq} (alkyl radical) to the underlying tissue. RNS are less affected by RH_{aq} . These fluences are also affected by the thickness of the liquid layer, which determines the residence time of radicals in the liquid. For thinner liquid layers, having shorter residence times, a significant fluence of OH_{aq} and $\text{HO}_{2\text{aq}}$, for example, are able to reach the underlying tissue. These species would otherwise be consumed in the formation of $\text{H}_2\text{O}_{2\text{aq}}$ and RNS ions.

Acknowledgment

This work was supported by the Department of Energy Office of Fusion Energy Science and the National Science Foundation.

References

- [1] Kong M G, Kroesen G, Morfill G, Nosenko T, Shimizu T, van Dijk J and Zimmermann J L 2009 *New J. Phys.* **11** 115012
- [2] Weltmann K-D, Kindel E, von Woedtkte T, Hähnel Ma, Stieber M and Brandenburg R 2010 *Pure Appl. Chem.* **82** 1123
- [3] Lloyd G, Friedman G, Jafri S, Schultz G, Fridman A and Harding K 2010 *Plasma Process. Polym.* **7** 194
- [4] Vandenbroucke A M, Morent R, De Geyter N and Leys C 2011 *J. Hazard. Mater.* **195** 30
- [5] Vandenbroucke A, Morent R, De Geyter N and Leys C 2011 *J. Adv. Oxid. Technol.* **14** 165
- [6] Mizuno A 2007 *Plasma Phys. Control. Fusion* **49** A1
- [7] Laroussi M and Akan T 2007 *Plasma Process. Polym.* **4** 777
- [8] Khacef A, Cormier J M and Pouvesle J M 2002 *J. Phys. D: Appl. Phys.* **35** 1491
- [9] Okubo M, Inoue M, Kuroki T and Yamamoto T 2005 *IEEE Trans. Industry Appl.* **41** 891
- [10] Jiang C, Mohamed A H, Stark R H, Yuan J H and Schoenbach K H 2005 *IEEE Trans. Plasma Sci.* **33** 1416
- [11] Fridman G, Peddinghaus M, Ayan H, Fridman A, Balasubramanian M, Gutsol A, Brooks A and Friedman G 2006 *Plasma Chem. Plasma Process.* **26** 425
- [12] Nastuta A V, Topala I, Grigoras C, Pohoata V and Popa G 2011 *J. Phys. D: Appl. Phys.* **44** 105204
- [13] Montie T C, Kelly-Wintenberg K and Roth J R 2000 *IEEE Trans. Plasma Sci.* **28** 41
- [14] Emmert S *et al* 2013 *Clin. Plasma Med.* **1** 24–9
- [15] Isbary G *et al* 2013 *Clin. Plasma Med.* **1** 25
- [16] Rhoades R A and Bell D R 2012 *Medical Physiology: Principles for Clinical Medicine* 4th edn (Baltimore, MD: Williams & Wilkins) pp 167–77
- [17] Schoenbach K, Kolb J, Xiao S, Sunao Katsuki, Y, Minamitani and Joshi R 2008 *Plasma Source Sci. Technol.* **17** 024010
- [18] Marinov I, Guaitella O, Rousseau A and Starikovskaia S M 2013 *Plasma Sources Sci. Technol.* **22** 042001

- [19] Strokin N A 2007 *High Energy Chem.* **41** 1
- [20] Emmin S S, Caminati S, Esposito B and Saracino M 2012 *Radiat. Phys. Chem.* **81** 1430
- [21] Krolla J H and Seinfeld J H 2008 *Atmos. Environ.* **42** 3593
- [22] Kroll J H, Ng N L, Murphy S M, Flagan R C and Seinfeld J H 2005 *Geophys. Res. Lett.* **32** L18808
- [23] Traylor M J, Pavlovich M J, Karim S, Hait P, Sakiyama Y, Clark D S and Graves D B 2011 *J. Phys. D: Appl. Phys.* **44** 472001
- [24] Sakiyama Y, Graves D B, Chang H, Shimizu T and Morfill G E 2012 *J. Phys. D: Appl. Phys.* **45** 425201
- [25] Ikawa S, Kitano K and Hamaguchi S 2010 *Plasma Process. Polym.* **7** 33
- [26] Fridman G, Brooks A D, Balasubramanian M, Fridman A, Gutsol A, Vasilets V N, Ayan H and Friedman G 2007 *Plasma Process. Polym.* **4** 370
- [27] van Gils C A J, Hofmann S, Boekema B K H L, Brandenburg R and Bruggeman P J 2013 *J. Phys. D: Appl. Phys.* **46** 175203
- [28] Hamaguchi S 2013 *AIP Conf. Proc.* **1545** 214
- [29] Machala Z, Tarabova B, Hensel K, Spetlikova E, Sikurova L and Lukes P 2013 *Plasma Process. Polym.* **10** 649
- [30] Xiong Z1, Robert E, Sarron V, Pouvesle J-M and Kushner M J 2012 *J. Phys. D: Appl. Phys.* **45** 275201
- [31] Babaeva N Y and Kushner M J 2013 *J. Phys. D: Appl. Phys.* **46** 025401
- [32] Sander R 1999 *Compilation of Henry's Law Constants for Inorganic and Organic Species of Potential Importance in Environmental Chemistry* www.henrys-law.org/henry.pdf
- [33] Mackay D and Shiu W Y 1981 *J. Phys. Chem. Ref. Data* **10** 1175
- [34] Parsons R 1990 *Chem. Rev.* **90** 813
- [35] *NIST Thermophysical Properties of Fluid Systems* <http://webbook.nist.gov/chemistry/fluid/>
- [36] Maddena K P and Mezyka S P 2011 *J. Phys. Chem. Ref. Data* **40** 023103
- [37] Chase W J and Hunt J W 1975 *J. Phys. Chem.* **79** 2835
- [38] *NDRL/NIST Solution Kinetics Database* <http://kinetics.nist.gov/solution/>
- [39] Pandis S N and Seinfeld J H 1989 *J. Geophys. Res.* **94** 1105
- [40] Hudson R D 1971 *Rev. Geophys. Space Phys.* **9** 305
- [41] Cox R A and Cole J A 1985 *Combust. Flame* **60** 109
- [42] Hotgne J and Bader H 1983 *Water Res.* **17** 173
- [43] Fry J L, Nizkorodov S A, Okumura M, Roehl C M, Francisco J S and Wennberg P O 2004 *J. Chem. Phys.* **121** 1432
- [44] Francea J L, Kinga M D and Lee-Taylorb J 2007 *Atmos. Environ.* **41** 5502
- [45] Neyens E and Baeyens J 2003 *J. Hazard. Mater.* **98** 33
- [46] Pavlovich M J, Chang H-W, Sakiyama Y, Clark D S and Graves D B 2013 *J. Phys. D: Appl. Phys.* **46** 145202
- [47] Ruscic B *et al* 2002 *Phys. J. Chem. A* **106** 2727
- [48] Szabó C, Ischiropoulos H and Radi R 2007 *Nature Rev. Drug Discovery* **6** 662
- [49] Pacher P, Beckman J S and Liaudet L 2007 *Physiol. Rev.* **87** 315
- [50] Reist M, Marshall K-A, Jenner P and Halliwell B 1998 *J. Neurochem.* **71** 2431
- [51] Laskin J D and Laskin D L 1999 *Cellular and Molecular Biology of Nitric Oxide* (Boca Raton, FL: CRC Press)
- [52] Atkinson R, Baulch D L, Cox R A, Crowley J N, Hampson R F, Hynes R G, Jenkin M E, Rossi M J and Troe J 2004 *Atmos. Chem. Phys.* **4** 1461
- [53] Nizkorodov S A and Wennberg P O 2002 *J. Phys. Chem.* **106** 855
- [54] Hippler H, Nasterlack S and Striebel F 2002 *Phys. Chem. Chem. Phys.* **4** 2959
- [55] Golden D M, Barker J R and Lohr L L 2003 *J. Phys. Chem. A* **107** 11057
- [56] Zhu R S and Lin M C 2003 *J. Chem. Phys.* **119** 10667
- [57] Oehmigen K, Hähnel M, Brandenburg R, Wilke Ch, Weltmann K-D and von Woedtke Th 2010 *Plasma Process. Polym.* **7** 250
- [58] Velpula N, Ugrappa S and Kodangal S 2013 *Int. J. Basic Clin. Pharmacol.* **2** 677
- [59] Denisov E, Chatgililoglu C, Shestakov A and Denisova T 2009 *Int. J. Chem. Kinet.* **41** 284
- [60] Fridman A and Friedman G 2013 *Plasma Medicine* (Oxford: Wiley) pp 115–20
- [61] Tresp H, Hammer M U, Winter J, Weltmann K-D and Reuter S 2013 *J. Phys. D: Appl. Phys.* **46** 435401
- [62] Babaeva N Yu and Kushner M J 2013 *J. Phys. D: Appl. Phys.* **46** 025401
- [63] Tresp H and Reuter S 2013 private communication